International Journal of Earth Sciences (2022) 111:53–84
https://doi.org/10.1007/s00531-021-02099-5

ORIGINAL PAPER

Tertiary monogenetic volcanism in the Gabal Marssous, Bahariya Depression, Western Desert, Egypt: implication for multi-phases, mafic scoria cone suite related to Red Sea rift in the Afro-Arabian realm

Ezz El Din Abdel Hakim Khalaf[1] · Mohamed Abdel Wahed[1] · Azeeza Maged[1] · Károly Németh[2,3]

Received: 7 March 2021 / Accepted: 10 August 2021 / Published online: 31 August 2021

Abstract
An integrated stratigraphic, sedimentological, volcanological, and geochemical studies were conducted for the first time on the eruptive products of the Marssous volcano, Bahariya Depression, Western Desert, Egypt. The rarity of complex volcanological studies in the west Red Sea rift makes these investigated volcanoes important as they offer a clue to the style of volcanism, eruptive environment and magma genesis during magmatism complimentary to those areas extensively studied in the Arabian Peninsula toward Syria and Eastern Turkey. The Marssous volcano is small monogenetic scoria cone that shows a polyphase feeding system, consisting of unconformable superimposed characteristic effusive-to-explosive eruptive units, suggesting a wide spectrum of diverse eruptive styles through a complex feeder network. On the basis of the sedimentological characteristics, field relationships, lava flow textures and granulometric indicators, five volcanic units have been identified from the base to top as (1) coherent porphyritic massive basalts (Bpm), (2) stratified tuff beds (Unit 1), (3) crude-bedded lapilli tuff beds with bombs (Unit 2), (4) massive agglutinate beds (composed of spatter and fluidal bombs) formed by lava fountains (Unit 3), (5) porphyritic vesicular basalts (Bpv), and (6) subvolcanic feeder intrusions. The degree of vesicularity and the size of the clasts increase from thin Unit 1 (ash to lapilli) through more thick Unit 2 (lapilli-bomb) to Unit 3 (breadcrusted scoriaceous bomb) as an indicative of an increased magma flux and the high eruptive energy together with an enlarged of degassing fragmentation. There is consequently a progressive evolution from an initial Phreatomagmatic explosive stage followed an initial effusive event to dry magmatic explosive (Strombolian & Hawaiian) and effusive eruptive styles in the later. With eruption progression, the external water to fuel Phreatomagmatism was diminished relatively early in the eruptions giving way to accumulate a pyorclastic fall deposition of Strombolian to Hawaiian lava-fountain episodes together with effusive eruptions, all together forming the majority of the pyroclastic and effusive successions of Gabal Marssous. These eruptive phases have happened during a continuous deposition without any time pauses in a short period of time as a result of a single cone-forming eruptions. The Marssous volcano shares resemblances in terms of inferred eruption style and structures with other scoria cones elsewhere in the broad regional context such as North Africa, Mediterranean province, and Arabian Peninsula, and thus provides an outstanding field laboratory to explore scoria cones architecture and growth from a global perspective. This volcano event is a key tectono-stratigraphic marker for an early manifestation, coinciding with the initiation of Red Sea rifting opening.

Keywords Spatter · Agglutinate · Spheriodal bombs · Lava flow · Strombolian · Hawaiian · Intraplate · Red Sea rift

Introduction

Monogenetic volcanoes are natural landforms formed by explosive and effusive eruptions both on land and on oceanic systems on Earth and they also exist on other planets (e.g., Németh and Kereszturi 2015). They prompted by the upsurge of small magma bunches within a distinct life time and without chronological hiatuses in their eruptive history (Cañón-Tapia 2016; Smith and Nemeth 2017).

✉ Ezz El Din Abdel Hakim Khalaf
e.2012_khalaf@hotmail.com; Ezzkhalaf2020@gmail.com

[1] Geology Department, Faculty of Science, Cairo University, Giza, Egypt

[2] School of Agriculture and Environment, Massey University, Palmerston North, New Zealand

[3] Institute of Earth Physics and Space Sciences, Sopron, Hungary

Their eruptive outputs can encompass numerous eruptive mechanisms, constructing diverse magma conducts such as effusive eruptions, or explosive (dry) fragmentation, e.g., Hawaiian or Strombolian eruptions, or as hydromagmatic (wet) fragmentation that may develop under dissimilar geodynamic conditions (Wohletz and Heiken 1992; Valentine and Gregg 2008; Kereszturi and Németh 2012a, b; Németh and Kósik 2020). They are characterized by wide spectrum of an edifice–building pyroclastic successions which mirror the type and grade of the interaction between internal- and external factors during the eruption process (Valentine and Gregg 2008; Kereszturi and Németh 2012a, b; Németh and Kereszturi 2015; Smith and Nemeth 2017). Processes such as shallow magma degassing, magma-water interaction, flow localization, abrupt decompression, and disequilibrium of magmatic foam all are responsible to govern explosive eruptions (Houghton et al. 2004). Eruptions of monogenetic volcanoes give valuable values for describing the tephra deposits, eruptive styles, morphologies, depositional processes, and genesis of the magmas that formed them in syn-eruptive and post-eruptive times, so providing vital idea about the eruptive mechanisms (e.g., Kereszturi et al. 2012; Murtagh and White 2013; Valentine et al. 2014; Kosik et al. 2016; Maro and Caffe 2016; Graettinger and Valentine 2017).

Monogenetic volcanoes can manifest in various forms from scoria cones to small shields and maar-diatremes, demonstrating the comprehensive scale of conceivable eruptive itineraries. Scoria cones are one of the well-known small-volume ($\leq$ 0.1 km^3) subaerial monogenetic volcanoes, which commonly preserve petrological features indicative to their rapid growth and short-lived life in geological sense (e.g., Valentine and Gregg 2008; Johnson et al. 2014; Németh and Kereszturi 2015; Pedrazzi et al. 2016). They formed in various tectonic settings including subduction, or continental rift, or mantle plume (Kienle et al. 1980; Cañón-Tapia 2016). Scoria cones vary in eruptive style from some mild intermittent or initial phreatomagmatic, through prevailing Strombolian to Hawaiian style explosions and mostly driven by mafic to intermediate magma (Fisher and Schmincke 1984; Kereszturi and Németh 2012a; Nemeth and Kosik 2020). These volcanoes provide key information about the the variability of the eruptive complexity and genesis of the magmas that formed them, as the magmatic processes involved during the course of the ascent of these magmas to the surface are commonly well preserved (e.g., Brenna et al. 2010, 2011; McGee and Smith 2016; Smith and Nemeth 2017). The scoria cones consist mainly of scoria accumulations (lapilli to bomb-size, ash used to be blown away) and are usually associated with lava flows (Walker 2000; Kereszturi and Németh 2012a; Risso et al. 2015). Recently, several studies on scoria cones have shown that their outputs reflect noteworthy verifications about their explosive eruption styles, facies architecture, and edifice geometry (Wood 1980; Valentine et al. 2005, 2007; Vespermann and Schmincke 2000; Guilbaud et al. 2009; Németh et al. 2011; Murcia et al. 2015). Older (1 My +) scoria cones are commonly dissected due to denudation and erosion exposing their inner architecture, providing invaluable assets to study shallow magma plumbing system linked to magmatic explosive eruption style-domianted small-volume volcano growth (Petronis et al. 2013, 2015, 2018). In this contribution, we document a complex, but still small-volume volcanic edifice from Egypt that provide clues to understand the growth of small-volume intraplate volcanoes.

No detailed data have previously been mentioned regarding the stratigraphy and lithofacies of Marssous volcano and its deposits. This work offers for the first time a full field-based documentation and description of facies architecture and eruptive mechanism included in the construction of Early Miocene scoria cone situated in the Gabal Marssous, Bahariya depression (BD), North Egypt, based on the stratigraphic successions and sedimentological characters of the rock protrusions. We selected Gabal Marssous to document a typical small-volume, but complex volcano formed predating the Red Sea rifting (Burke 1996; Bosworth and William 2015; Ligi et al. 2018) in its African rift shoulder side for the following reasons: (1) Gabal Marrsous has spectacularly well-preserved crescent morphology, (2) it is an outstanding set of outcrops exposing various mafic pyroclastic deposits, with excellent accessibility, not having counterpart in the entire region; (3) it has rhythmic layers of pyroclastic units recording repeated explosive and effusive phases, hence demonstrating a distinctive change in eruptive styles; and (4) lava flows are recognized in Gabal Marssous compared with the predominant subvolcanic intrusions in the northern areas of the Bahariya depression (Khalaf et al. 2019). So, the present work aims to (i) elucidate and describe the lithofacies characteristics of the exposed volcanic deposits from the eroded Marssous volcano, BD based on stratigraphy, sedimentology, petrography, and SEM microscopy, (ii) clarify the evolutionary history of the scoria cone, (iii) offer insight about processes-controlled emplacement mechanism and the dynamics of the plumbing system to understand its eruptive styles, and (iv) compare the studied volcanics with the equivalent rock units worldwide. The selected scoria cone in the Gabal Marssous is a representative volcano because it displays effusive to explosive phases, giving a good chance to comprehend the lateral and vertical facies distribution of the composite eruptions on mafic scoria cone that can be prolonged to other scoria cones elsewhere.

Geological backgrounds

Regional stratigraphy and tectonic framework

The Red Sea rift is an astonishing model of a broad extensional zone separating African from the Arabian plate. This

NNW-SSE trending rift extends about 2200 km in length and its opening initiated at 30 Ma (Roobol and Camp 1991; Camp and Roobol 1992; Bosworth et al 2005; Bryan and Ernst 2008). The Red Sea rift is associated with three volcanic phases involving (i) pre-rift volcanism (46–34 Ma); (ii) syn-rift volcanism (30–25 Ma), and (iii) post-rift volcanism (< 20 Ma) (Bosworth and Stockli 2016). The southern Red Sea region involve voluminous volcanic phases which extend from Afar and Yemen to Saudi Arabia (Harret volcanic fields), Jordan, and Syria. In contrast, the northern Red Sea province involving Egypt has less voluminous volcanism and less evidence for doming (Camp and Roobol 1992; Shaw et al. 1968). There is a change in source for these volcanoes from plume-derived volcanism underneath the Afar and Arabian plate (Ilani et al. 2001) to upper lithospheric mantle (Schilling et al. 1992; Volker et al. 1997).

Polyphase extensional and inversion tectonics affected the African plate during Mesozoic and Cenozoic Eras (Bosworth 1992; Bosworth et al. 2008). NW-SE compressional phase affected Late Cretaceous-Early Tertiary basins (Fig. 1A). This basin inversion produced the Syrian Arc System (SAS) which extends from Syria to central Egypt through the Western Desert of Egypt (Guiraud and Bosworth 1997; Guiraud et al. 2005). A great number of E–W and NE–SW trending sedimentary basins which are delimited by folds and tectonic horsts belonging to SAS are exposed in North Egypt (Fig. 1A), especially in the BD (Said 1962, 1990; Sehim 1993; Guiraud et al. 2005; Bosworth et al. 2008). Most of these basins were occupied by diverse rocks of marine to nonmarine sedimentary rocks together with volcanic and volcaniclastic deposits directly related to Red Sea rift opening.

The Bahariya depression is positioned in the Western Desert, 320 km southwest of Cairo, delimited between latitudes 27°48′ N and 28°30′ N and longitudes 28°35′ E and 29°10′ E, covering an area of about 1800 km^2. It attains a width of about 42 km with a chief axis running southwest-northeast for around 90 km, displaying a large oval shape. The excavation of the BD was accredited to aeolian and karst routes facilitated by the structural alignment (Said 1962; El Aref et al. 1987, 1991). The stratigraphic record in the BD involves sedimentary strata of Cenomanian to Lutetian (Said 1990). Cenomanian clastic sediments (Bahariya Formation) appear on the basin floor, while Eocene carbonates occupy the escarpments of the BD (Fig. 1C, D).The former is characterized by large concentric structures (CS) along the Mid Bahariya fault (Fig. 1C, Mazzini et al. 2019). The BD is characterized by abundant inselbergs of Upper Cretaceous rocks, consisting of (a) ferricrite crusts forming the Black Desert (El Aref et al. 2017), (b) karstic Campanian and Eocene carbonates (El Aref et al. 2017), or (c) Miocene lava flows and subvolcanic intrusions (Bosworth et al. 2015; Khalaf and Hammed 2016).

The BD was subjected to several structural processes during Upper Cretaceous, Post-Middle Eocene, and Middle Miocene periods (Moustafa et al. 2003). During Late Cretaceous period, the BD was affected by enechelon pattern of double-plunging anticlines and synclines along NE-dextral wrench faults of the compressional SAS (Fig. 1A; Sehim 1993; Moustafa et al. 2003; El Ghamry et al. 2020). The latter authors concluded that these wrench deformations intermittently rejuvenated during Late Eocene/Miocene period that are well exposed with three main E-NE-oriented fault systems involving Northern, Mid- and Southern Bahariya fault systems pronounced across the BD (Fig.2). During the Middle Miocene, the BD was influenced by a chain of NNW-and NW-trending normal faults forming grabens (1–2 km wide) and accompanied by eruption of lava flows as well as subvolcanic intrusions (Moustafa et al., 2003; Bosworth et al., 2015). This volcanic phase was most probably linked to the Gulf of Suez and Red Sea Rift during Early Miocene (Moustafa et al., 2003). Abdel Aal (1998) approved that the basalts of west Cairo were linked to rifting during Early Miocene and decided that the magma outlets were controlled by E–W and NW-trending fault systems.

The Bahariya volcanoes

In North Egypt, the Cenozoic volcanoes occupy pervasive districts (15,000–25,000 km^2). They are well exposed in Bahariya depression, Gabal Qatrani, west Cairo, Cairo-Suez road, and Sinai Peninsula as well as Minya and Samalut along River Nile. Their outcrops occur in the form of mafic scoria/cinder cones, lava flows, and subvolcanic intrusions that were erupted between 27 and 20 Ma (Meneisy 1990; Baldridge et al. 1991; Endress et al. 2009, 2011). The Bahariya volcanoes (BV) represent short-lived monogenetic volcanoes that are mostly dispersed in the Northwestern Desert of Egypt. The latter suffered intense deformation and magmatism during Oligocene-Miocene epoch. The BV are well exposed within the northern block of the Mid-Bahariya fault and form the Gabals of El-Mandisha, El-Mayesra, El-Agoz, El-Hefhuf, and El-Marssous (Fig. 1B). These occurrences are chiefly characterized by wide varieties of lithofacies involving pyroclastics, lava flows, peperitic breccias and sills/dikes (Khalaf et al. 2019). The former two facies are well exposed in the Gabal Marssous, while lava flows, peperitic breccias and their feeder sills/dikes form the main constituents of El-Mandisha, El-Mayesra, El-Agoz, and El-Hefhuf (Fig. 1B). These volcanic exposures occur as isolated masses with no direct contact between them that overlie Bahariya and El-Hefhuf Formations of Upper Cretaceous (Fig. 1D). Based on ^{40}Ar/^{39}Ar dating, volcanism occured between 23 and 20 Ma (e.g., Bosworth et al. 2015). New ^{40}Ar/^{39}Ar dating revealed age of 23.71 ± 0.06 and 23.73 ± 0.01 Ma for the eruption of the BV (Khalaf and Sano 2020).

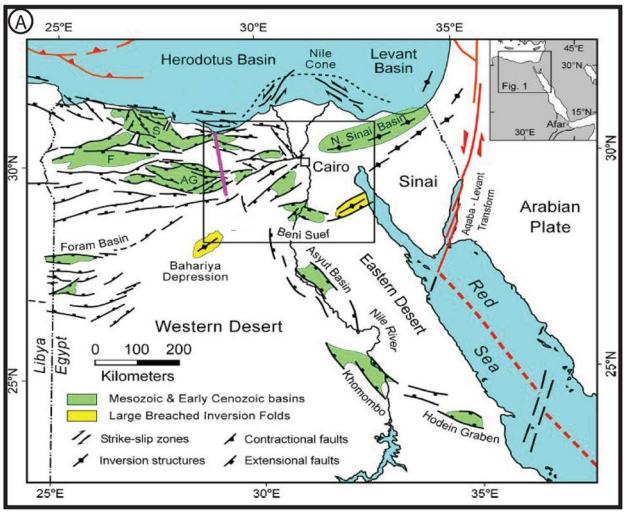
A
Herodotus Basin
Nile Cone
Levant Basin
N. Sinai Basin
Cairo
Sinai
Arabian Plate
Aqaba - Levant Transform
Beni Suef
Foram Basin
Bahariya Depression
Asyut Basin
Eastern Desert
Nile River
Red Sea
Western Desert
Libya
Egypt
Khomombo
Hodein Graben
Kilometers
Mesozoic & Early Cenozoic basins
Large Breached Inversion Folds
Strike-slip zones
Contractional faults
Inversion structures
Extensional faults

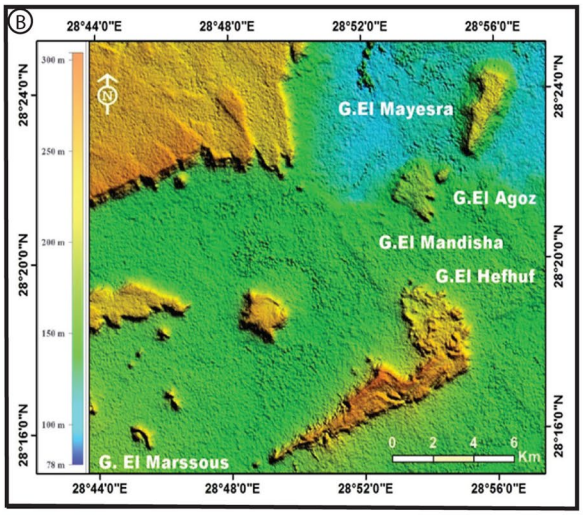
B
G.El Mayesra
G.El Agoz
G.El Mandisha
G.El Hefhuf
G. El Marssous
Km

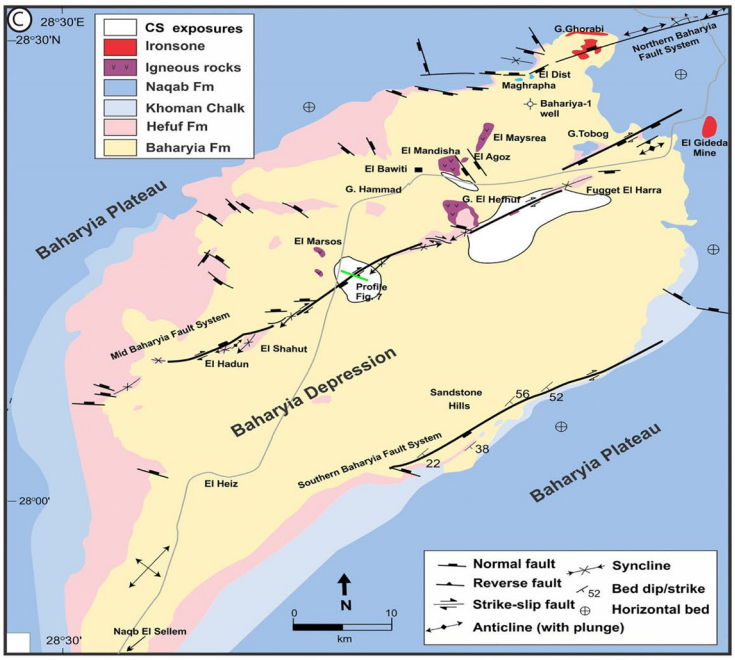
C
CS exposures
Ironsone
Igneous rocks
Naqab Fm
Khoman Chalk
Hefuf Fm
Baharyia Fm
Baharyia Plateau
Baharyia Depression
G.Ghorabi
Northern Baharyia Fault System
El Dist
Maghrapha
Bahariya-1 well
El Maysrea
G.Tobog
El Gideda Mine
El Mandisha
El Agoz
El Bawiti
G. Hammad
G. El Hefhuf
Fugget El Harra
El Marsos
Profile Fig. 7
Mid Baharyia Fault System
El Shahut
El Hadun
Sandstone Hills
Southern Baharyia Fault System
El Heiz
Naqb El Sellem
Normal fault
Reverse fault
Strike-slip fault
Anticline (with plunge)
Syncline
Bed dip/strike
Horizontal bed

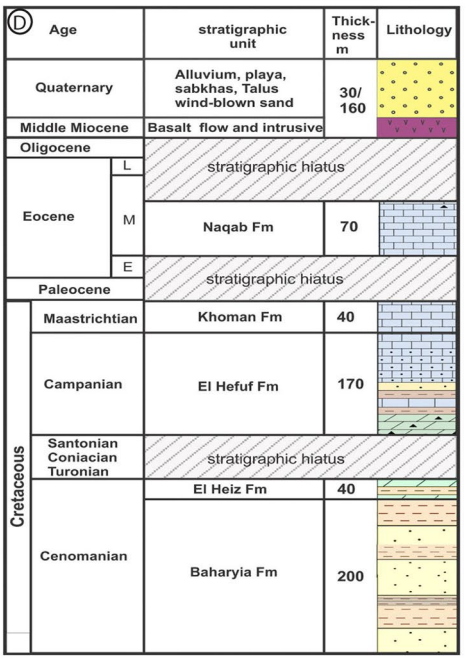
D
Age
stratigraphic unit
Thick-ness m
Lithology
Quaternary
Alluvium, playa, sabkhas, Talus wind-blown sand
30/ 160
Middle Miocene
Basalt flow and intrusive
Oligocene
Eocene
L
M
E
stratigraphic hiatus
Naqab Fm
70
Paleocene
Cretaceous
Maastrichtian
Khoman Fm
40
Campanian
El Hefuf Fm
170
Santonian Coniacian Turonian
Cenomanian
El Heiz Fm
40
Baharyia Fm
200


E


F
Lava 1
Lava 1
lava 2
Lava 1
Pyroclastics
Lava 1
Pyroclastics
Bahariya Fm
Bahariya Fm
Bahariya Fm

◂**Fig. 1** **A** The Mesozoic and Early Cenozoic basins of northern and central Egypt; *AG* Abu Gharadig basin, *F* Faghur basin, *S* Shushan basin (after Bosworth et al. 2015). **B** Shaded relief Digital Elevation Model (Alos-Palsar DEM data, 12.5 m resolution) showing the topography of the investigated Bahariya volcanics. **C**, **D** The geological map and the stratigraphic section of the Bahariya Oasis (after Moustafa et al. 2003). **E** Flat and broad circular depression of the Marssous scoria cone. **F** Panorama showing the eastern parts of Gabal Marssous. The rock sequence starts by the Bahariya Formation at the base followed up section by lava1, pyroclastic deposits, and lava 2 at the topsection. Photo looking west. Note NE-trending normal faults cut the Marssous sequence forming grabren structure

These volcanic exposures have diverse periods of intensive small-volume mafic volcanism (Khalaf and Hammed 2016), as a result of outpouring of asthenospheric mantle over regional-scale (e.g., Lustrino and Wilson 2007; Mazzarini et al. 2013; Rooney et al. 2014; Ma et al. 2016; Khalaf and Sano 2020).

The Marssous scoria cone is one of the Neogene volcanoes exposed along the north section of the Western Desert during opening of the Red Sea. This scoria cone situated at the western flank of the BD (Fig. 1C), 13 km southwest of the Bawiti town, represents Miocene subaerial small-volume volcanic episode recorded in North Egypt. It is settled inside the main Bahariya depression close to the escarpment of the Eocene plateau. The Marssous cone forms broad semicircular volcanic depression (Fig. 2). Its chief exposure displays a semi-circular shape within an incomplete ring having rugged landscape (Fig. 2A–C). The volcanic cone is asymmetrically elongated NW–SE, ~1500 m long and 1000 m wide, covering an area of about 4.0 km^2 and 100 m high overlying Bahariya Formation without clear metamorphic effect at the contact between them (Fig. 1E, F). The eastern flank of the scoria cone displays a fan-shaped morphology compared with circular-shaped topography in its western part (Fig. 3A). Most of the rock surfaces are covered by Quaternary aeolian sand (Fig. 3A). Along the inner slopes of the cone exposed volcanic rocks show a dip angle of 60°–80°. The outcrops of the cone are dissected by numerous fractures/faults. Gullies and ravines together produced pronounced valley incisions, cone segmentation and truncations. These faults are NW and NE-trending dip-slip normal faults (Fig. 1D) with pitches of slickenside lineation around 80°–90° (Fig. 3B). The circular faults are the most common recorded types as evidenced by a circular valley bounding the main cone from its northern, northeastern, and eastern parts (Fig. 3D) and the displacement of the upper lava downwards towards the cone with a downthrown side towards the main cone. The Marssous cone preserves mafic pyroclastic deposits, two distinct lava flows and dikes (Figs. 1F, 2D). The pyroclastic rocks are sandwiched between the lava flows (Fig. 2D). The lava flows are slightly tilted radially away from the cone and show considerable dip close to faults. The whole succession is unconformably capping the Upper Cretaceous Bahariya formation which is remarkably tilted under the nearly horizontal flows (Fig. 1F). 20.66 ± 0.55 Ma is assigned to the Marssous volcanoes based on K/Ar dating (Agostini et al. 2016).

Methology and terminology

The rock lithofacies were described in the field based on lithological, sedimentological, textural, and primary structures characteristics. Two stratigraphic sections (Figs. 4, 5) were documented at the east and west of the scoria cone (Fig. 2C). Field mapping was done to recognise volcanic lithofacies, clast size, textural composition, pyroclast constituents, deposit characteristics, and alteration type (Sohn and Chough 1992; Németh and Martin 2007). Petrographic features for more than 50 thin sections were investigated by optical microscopy to document compositional characteristics of the examined volcanoes. Petrographic features are further studied by Scanning Electron Microscopy (SEM). SEM observations were made using a JEOL JXA-898A electron prob microanalyzer-JEOL-Japan operating at 30 kV at the Egyptian Geological Survey. Whole-rock analyses of five lavas and three scoria samples were done at the National Museum of Nature and Science, Tsuskuba, Japan using XRF and ICP-MS techniques (Supplementary Table 1). In this paper, pyroclastic deposits were classified based on the granulometry scheme after Sohn and Chough (1992). The facies description of the coherent lava flows was based on the composition followed by the fabric and lava structures (e.g., massive, porphyritic, aphanitic, vesicular) as suggested by McPhie et al. (1993). The lithofacies were assembled in facies associations involving genetically related rock units (Collinson 1969, 1996; Dalrymple 2010).

Results

Stratigraphy and facies association

This study offers for the first time a detailed field-based documentation and description of facies architecture and eruptive mechanism involved in the formation of the Marssous volcanoes based on their sedimentological and textural characteristics. Eleven lithofacies were documented for the Marssous volcano which are divided into three coherent and eight volcaniclastics, following an analogous systematic adoption by Sohn and Chough (1992) and Rossetti et al. (2014). They are grouped into three major facies associations including pahoehoe lava flows, proximal pyroclastics, and coherent subvolcanic intrusions. The rock lithofacies are defined and interpreted in Table 1.

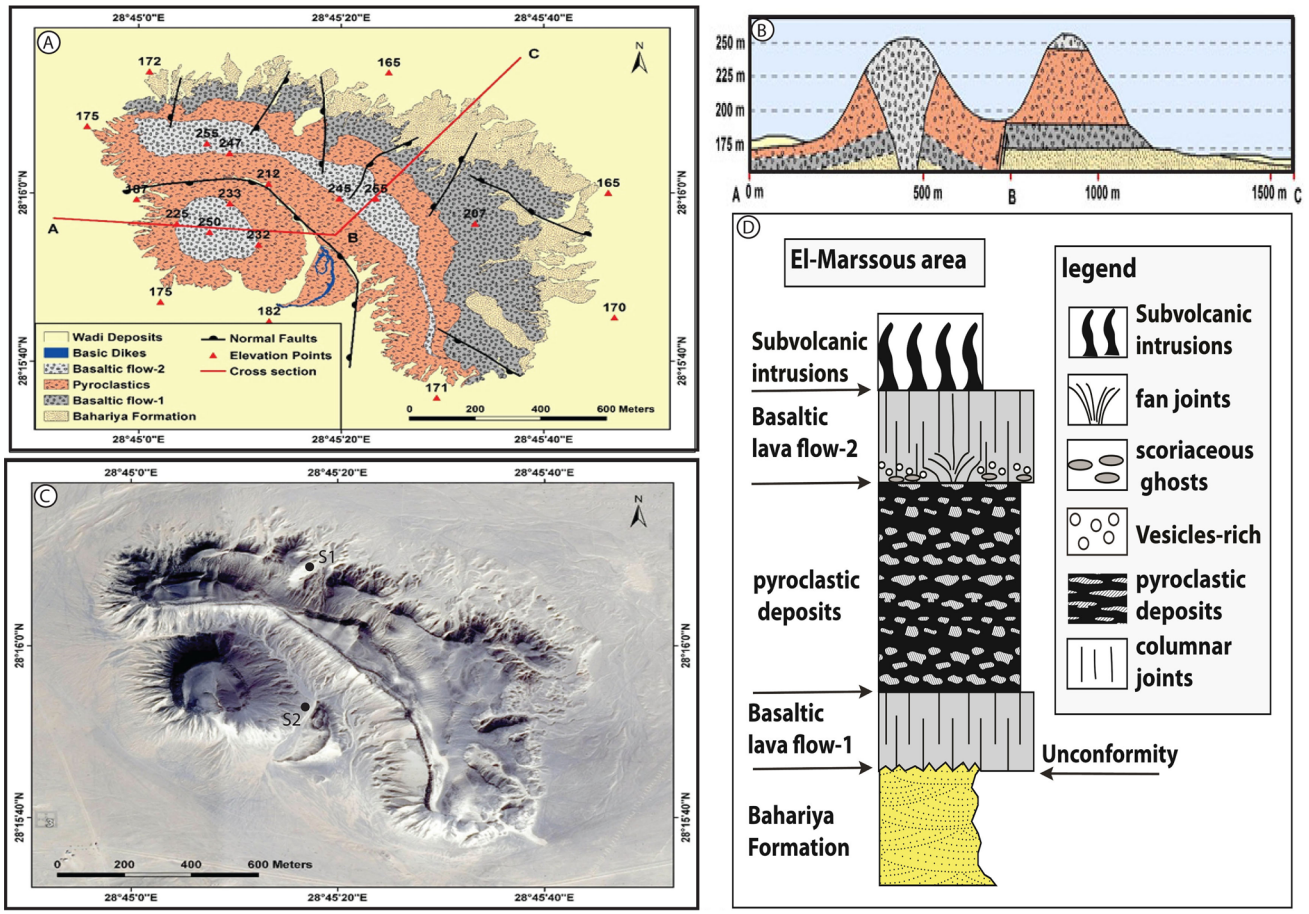

Fig. 2 **A** Detailed geologic map of Gabal Marssous area. **B** The cross section showing field relationship of the studied rock units at Marssous scoria cone. **C** High resolution Google Earth satellite image (0.5 m/pixel) showing crescent-shaped topography of Marssous scoria cone. Note the situation of two stratigraphic sections for facies analysis (S1 & S2). **D** Stratigraphic column of the rock units in Gabal Marssous area

Pahoehoe lava flows

Pahoehoe lava flows spread east and west of the scoria cone, covering an area of ~ 4 km^2. They form two stratigraphic packages that underlie and cap the pyroclastic deposits, characterizing the Gabal Marssous scoria cone (Figs. 1E, 2). The lavas having a thickness of about 25 m, represent about 40% of preserved volcanic products of the scoria cone. The high thickness suggests the lavas filled some gullies or small valley. The lavas are considered as a simple lava flow (Walker 1971; Pinkerton and Sparks 1976; Murcia and Németh 2020). On the basis of texture and vesiculation, two facies types are identified east and south of the scoria cone: massive porphyritic basalt (Bpm) and vesicular porphyritic basalt (Bpv).

Massive porphyritic basalts (Bpm) *Description* This facies forms irregular unconformable contact with the underlying Bahariya Formation (Fig. 1F). The latter separates from the overlying lava flow (lava 1) along thin peperitic breccias at the eastern ridge of the scoria cone. This brecciated zone, 5–10 cm thick, is clast-supported and contains 4–15 cm large basaltic clasts embedded in sandy matrix (Fig. 3C). This lava facies is massive, dark gray in color, poorly vesicular, aphanitic coherent flow and attains 15–20 m in thickness. The lava architecture is marked by low slope. Its base is 1–2 m thick with some spherical vesicles (3–5 mm in size) that decline at the flow top. The flow core, 10–15 m in thickness, is characterized by thin platy horizontal (3–5 cm) and colonnade joints which range in width from 0.7 to 1 m. This flow is crossed by a complex system of fractures. The platy joints are near horizontal in cross-section view, dipping frequently ~10°. Low angle fractures with 15°–30° dip are common in some outcrops (Fig. 3E). The flow top has smooth convolute surfaces (Fig. 4), occupied by loose fragments displaying ball shape and is reddish-brown in color, due to the effect of weathering and alteration.

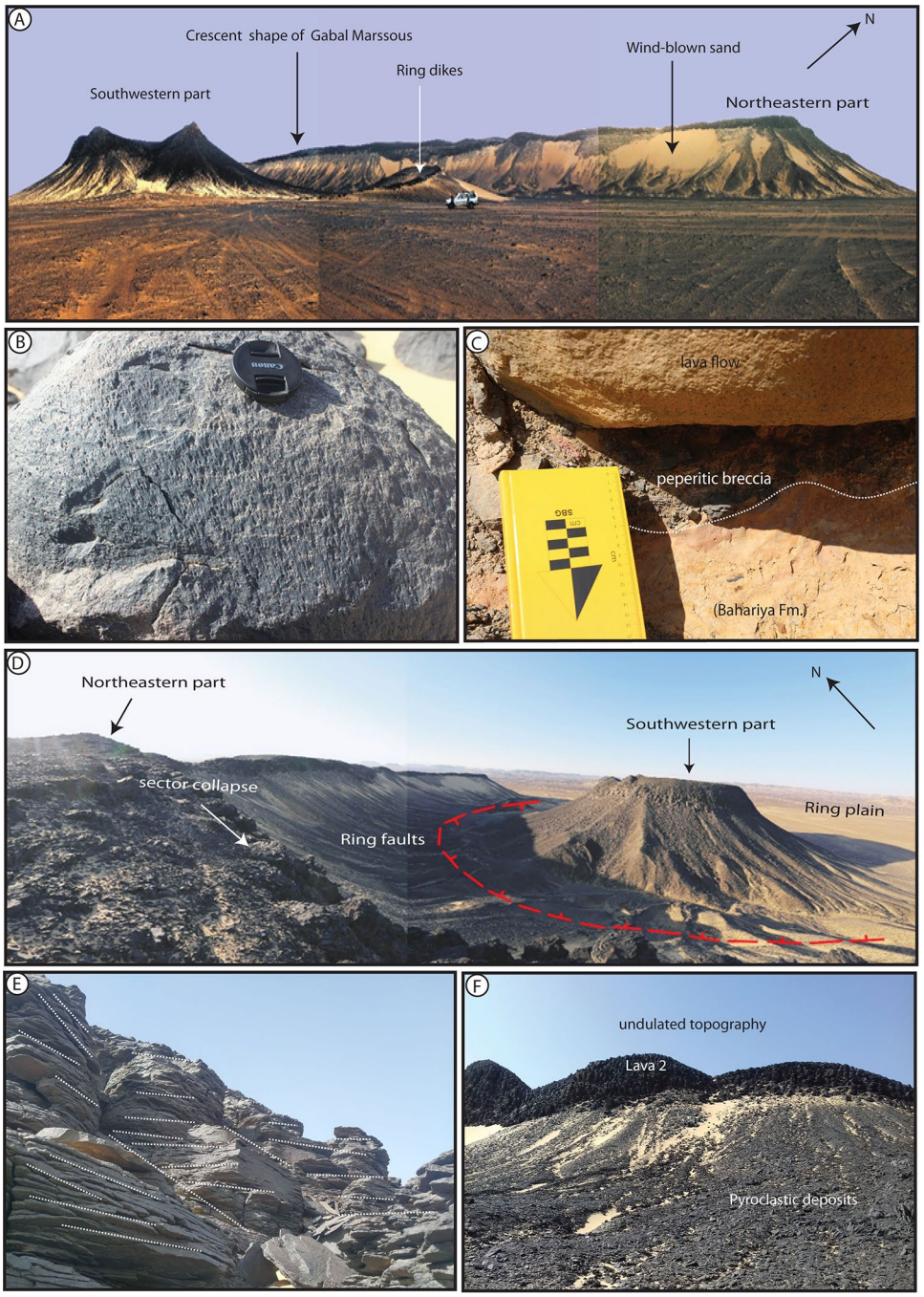

Fig. 3 **A** Panorama showing semi-circular morphology of Gabal Marssous. Photo looking northwest. **B** Well-developed slickensides in a basalt fragment found along one of the normal faults affecting the eastern parts of the area. **C** Thin peperitic breccias delineated along the contact between Bahariya Formation and lava 1. **D** Panorama showing the northwestern side of Gabal Marssous illustrating the ring fault surrounding the main cone. Photo looking southeast. **E** Network of horizontal and low angle fractures/joints (5°–20°) crosscut massive porphyritic basalts of Pahoehoe flow (Bpm). **F** Undulated topography of vesicular porphyritic basalts of Pahoehoe flow (Bpv)

Vesicular porphyritic basalts (Bpv) *Description* This facies, 5–25 m thick, characterizes the eastern/southern part of the scoria cone and the Hefheufe area. Along the west ridge of the scoria cone, the flows of this facies unconformable overlie the pyroclastic deposits (Fig. 4) with undulated topography (Fig. 3F) along a planar, transitional diffuse brecciated contact (Fig. 6A). The latter, up to 60 cm in thick, is clast-supported, consisting of tephra and lava clasts set in schistose matrix.The lava flows display heterogeneous texture that is characterized by existence of irregular scoriaceous fragmental patches (Fig. 6B) especially close to the transitional contact with the pyroclastics deposit. These patches have variable shape and it is highly enriched in spherical vesicles. Away from this contact, the remaining lava flows are black gey, massive, homogeneous, isotropic, and aphyric in texture. These flows are enriched in spherical vesicles (Fig. 6C). The 15–20-m-thick core of the lava is jointed into 30–40 cm wide columns with fan or colonnade arrangement, and it is capped by 5-m-thick blocky domain (Fig. 6D). Classic

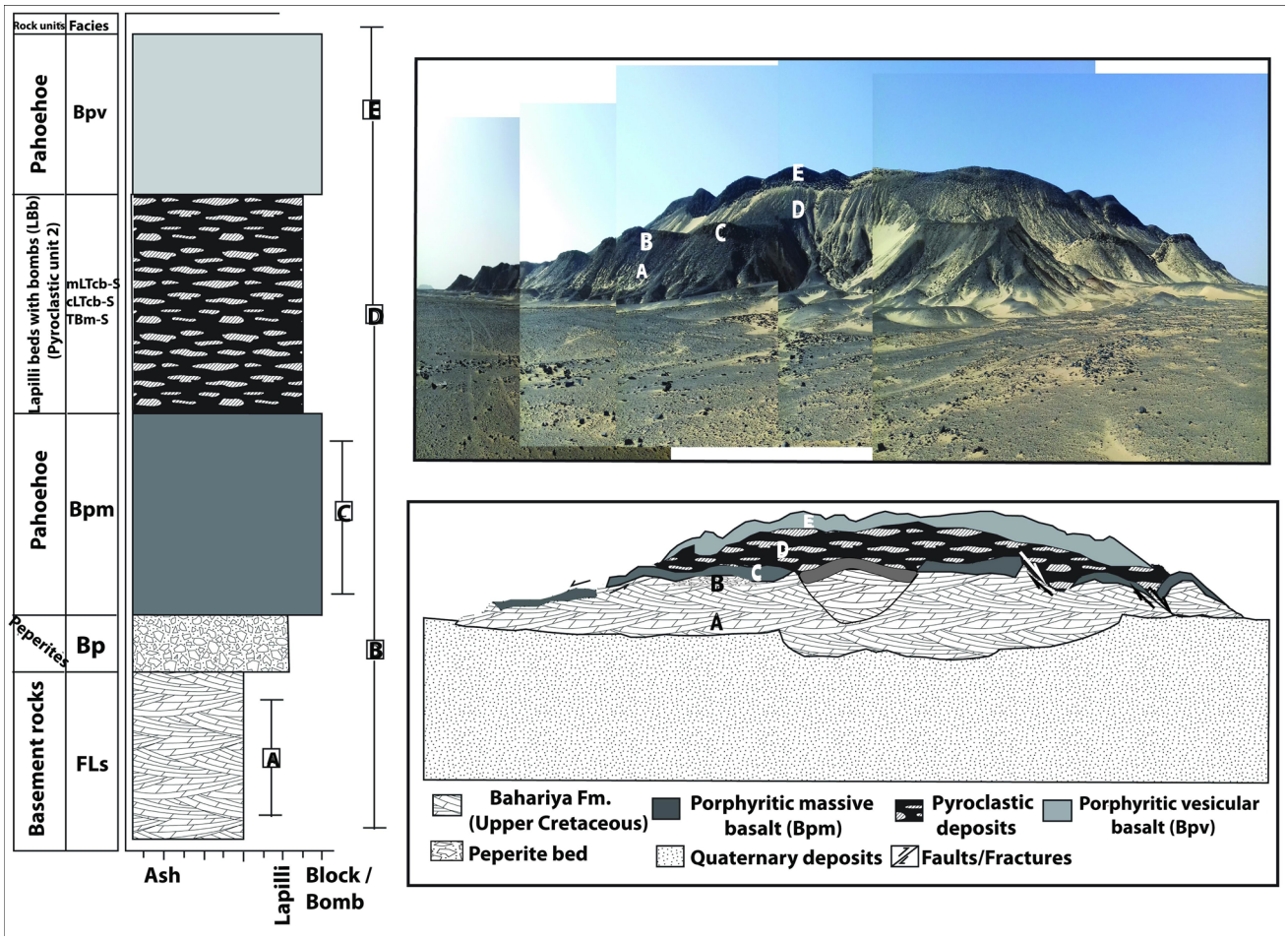

Fig. 4 Schematic stratigraphic section along the east scoria cone. **A** Fluviolacustrine sediments of Bahariya Fm (lithofacies A) represent the basement rocks. **B** Peperitic breccias (Bp, lithofacies B). **C** Massive porphyritic basalts (Bpm, lithofacies C), **D** Lapilli beds with bombs (LBb) of pyroclastic unit 2 (lithofacies D) comprises three lithofacies involving crude bedded medium lapilli tuff-Strombolian (mLTcb-S), crude bedded coarse lapilli tuff-Strombolian (cLTcb-S), and massive tuff breccias-Strombolian (TBm-S). **E** Vesicular porphyritic basalts of Pahoehoe flow (Bpv, lithofacies E). See Fig. (3C) for location

volcanic structures including lava balls (Fig. 6D) and ropy pahoehoe can be identified (Fig. 3F). The lava flows and the underlying pyroclastics are intruded by feeder dike associated with extensive alteration zone (Fig. 6D). Rock samples from both Bpm and Bpv have the same mineral composition. They are massive, porphyritic, holocrystalline, consisted of 18–26% phenocrysts involving olivine, and clinopyroxene embedded in plagioclase laths-rich groundmass (Fig. 6F). Subhedral crystals of olivine with partial to complete alteration especially along fractures and crystal margins have been observed (Fig. 6F). Clinopyroxene phenocrysts are even more abundant than those of olivine.They form subhedral crystals, with pink pleochroism, displaying characteristic oscillatory and hour glass or sector zoning (Fig. 6G). Olivine-clinopyroxene glomerocrysts are enclosed in fine-grained intersertal, pilotaxitic, to flow intergranular matrix, comprising variable amounts of plagioclase laths, clinopyroxene prisms, and skeletal acicular ilmenite rods.

Promixal pyroclastic rocks

The pyroclastics rocks, up to 80 m thick, represent the dominant rock types through the whole area of the Marssous volcano (Fig. 2A). Their deposits cover the pre–existing topography. In spite of the common inaccessibility of the pyroclastic deposits, they have been described in two distinct sites (Figs. 4, 5), situated on the eastern and western ridges of the cone (Fig. 2C). The distance between the two sites is about 1000 m. The faults-controlled contact separates between the two sites involving thick sequence of pyroclastic rocks and jointed lava flows (Fig. 2A, B). Their beds usually dip south-westwards by 60°. The rock outcrops of the pyroclastic deposits display a discrete color

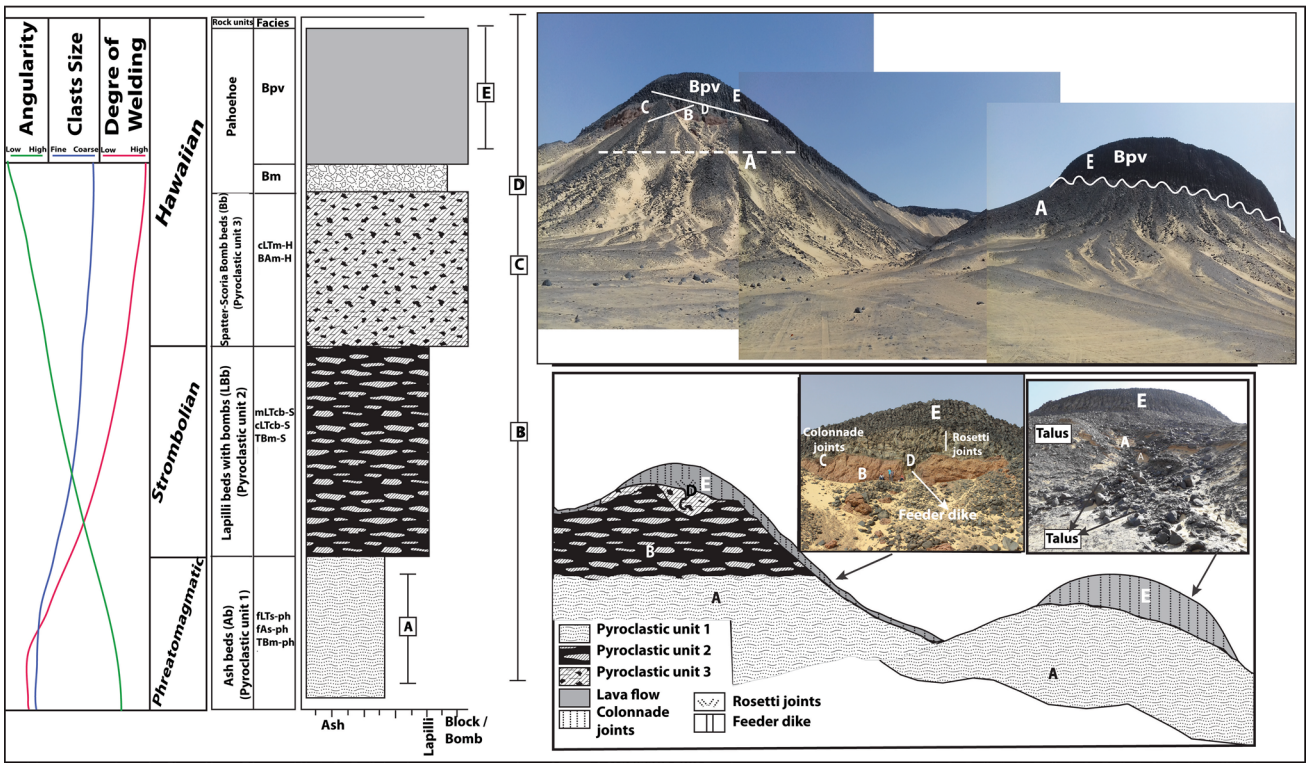

Fig. 5 Schematic stratigraphic section along the west scoria cone. **A** Tuff beds (Tb) of pyroclastic Unit 1 contains three lithofacies involving stratified fine lapilli tuff-Phreatomagmatism (fLTs-Ph), stratified fine tuff-Phreatomagmatism (fts-Ph), and masstive tuff breccias-Phreatomagmatism (TBm-Ph). **B** Lapilli beds with bombs (LBb) of pyroclastic Unit 2 comprises three lithofacies involving crude bedded medium lapilli tuff-Strombolian (mLTcb-S), crude bedded coarse lapilli tuff-Strombolian (cLTcb-S), and massive tuff breccias-Strombolian (TBm-S). **E**, **C** Spatter-scoria bomb beds (Bb) of pyroclastic Unit 3 include two lithofacies involving massive coarse lapilli tuff-Hawaiian (cLTm-H) and massive tuff breccias-Hawaiian (TBm-H). **D** Massive breccia (Bm). **E** Vesicular porphyritic basalts of Pahoehoe flow (Bpv). See Fig. 3C for location. In both sections, the grain size variation, angularity, and degree of welding for each eruptive phase have been represented

zonations ranging from whitish grey through brown to red at the topmost. They are hetrogeneous, comprising massive to crude bedded, matrix-to clast-support, weakly to highly agglutinated, poorly to moderately sorted, tuff to lapilli and bombs that become coarser near the top (Fig. 5). So, three main pyroclastic units were identified and discriminated in ascending order based on the sedimentological characteristics and color difference between the units, namely lower Unit 1 (whitish grey), tuff beds (Tb), middle Unit 2 (brown), lapillituff beds with bombs (LBb), and upper Unit 3 (red) spatter-scoria bomb beds (Bb) (Fig. 5). Universally the relative abundances of the tuff beds decreses up-section and consequently lapillituff and agglomeratic beds become progressively more dominant in upsection. At all the studied sites, the pyroclastic deposits show significant variation in color, thickness, and lithological features. Unit 1 occurs at the base, while Unit 3 occupy the top part of the scoria cone (Fig. 5). On the western side of the scoria cone, all three units occur, but on the eastern side, only Unit 2 is present (Fig. 4). The boundaries between these units are gradational to sharp that are characterized by "well-developed unconformity surface", signifying main fluctuations in the sedimentary and eruptive regime of the volcanic system.

Unit 1: tuff beds (Tb) *Description* This unit, up to 25 m thick, underlying the lava flows along unconformable surface, forms the bottom of the scoria cone at the western part. (Figs. 5, 7A). Its base is unexposed, due to thick alluvium/talus cover (Fig. 7A). The boundary between Unit 1 and overlying Unit 2 is uncertain and unclear because most of its unravelling borders are covered by aeolian sand. The facies of Unit 1 is stratified or planar bedded, poorly sorted, and matrix-supported (Fig. 7A, B). The bedding of the former dips 20°–50° towards west. Its outcrops are organized in centimeter- to decimeter-thick stacked beds that vary from fine tuff to fine lapilli tuff grading to tuff breccia (e.g., fT to fLT and TB on Fig. 7A, B). The contacts between the lapilli tuff and tuff layers are gradational and difuse, without signs of erosional surfaces. The thickness of the beds is abruptly changing over short distances, but obvious single beds are in the range of centimetres to some meters thick. The sequence of the Unit 1 is formed by moderately to weakly indurated,

Table 1 Facies characteristics at Gabal Marssous, Western Desert, Egypt

Facies association	Lithofacies	Facies code	Description	Interpretation
Pahoehoe lava flows	Massive porphyritic basalt	Bpm	Massive, dark gray, aphyric, poorly vesicular, coherent flow and attains 15–20 m in thickness. Platy horizontal and colonnade joints are common	Low effusive rate and low viscosity with even flat topography
	Vesicular porphyritic basalt	Bpv	Massive, black gey, aphyric, vesicles-rich, forms heterogeneous scoriaceous zone enriched in ghost clasts close to pyroclastics contact. fan/colonnade-joints are common	Fast cooling lavas with high rate of nucleation and low rate of crystal crystallization
Proximal pyroclastic rocks	Tuff beds	Tb	stratified, white grey, matrix-supported, poorly sorted, angular to subangular,composed of thin layers of ungraded to normally graded fine lapilli tuff (fLT) and fine tuff (fT) beds grading to Tuff breccia (TB) with characteristically planar low angle cross and dune bedding structure	Pyroclastic density currents (PDCs), as the result of explosive magma-water interaction, forming phreatomagmatic eruptions
	Lapilli tuff beds with bombs	LBb	Crude bedded, brown, clast supported, moderately sorted, subangular to subrounded, composed of decimeter- to meter-thick medium to coarse lapilli tuff (mLTcb & cLTcb) grading to massive tuff breccia (TBm). Impact sags and moderate to high vesiculation of juvenile clasts are verified	Ballistics and air fallout deposit derived from Strombolian-style eruptions
	Spatter-scoria bomb beds	Bb	Massive, red, clast-supported, moderately sorted, highly welded, subrounded to rounded, composed of coarse lapilli tuff (cLT) grading to agglomerate (BA). spheroidal scoriaceous lapilli/bombs having cauliflower and/or ropy surface textures are common	Spatter deposits derived from Hawaiian-style lava fountaining
Coherent subvolcanic intrusions	Dikes		Massive, black, poorly vesicular, aphyric, curved subvertical to vertical coherent/pyroclastic dikes with ring outcrops in some locations	Feeder dikes formed during waning phases and terminations of the eruptions

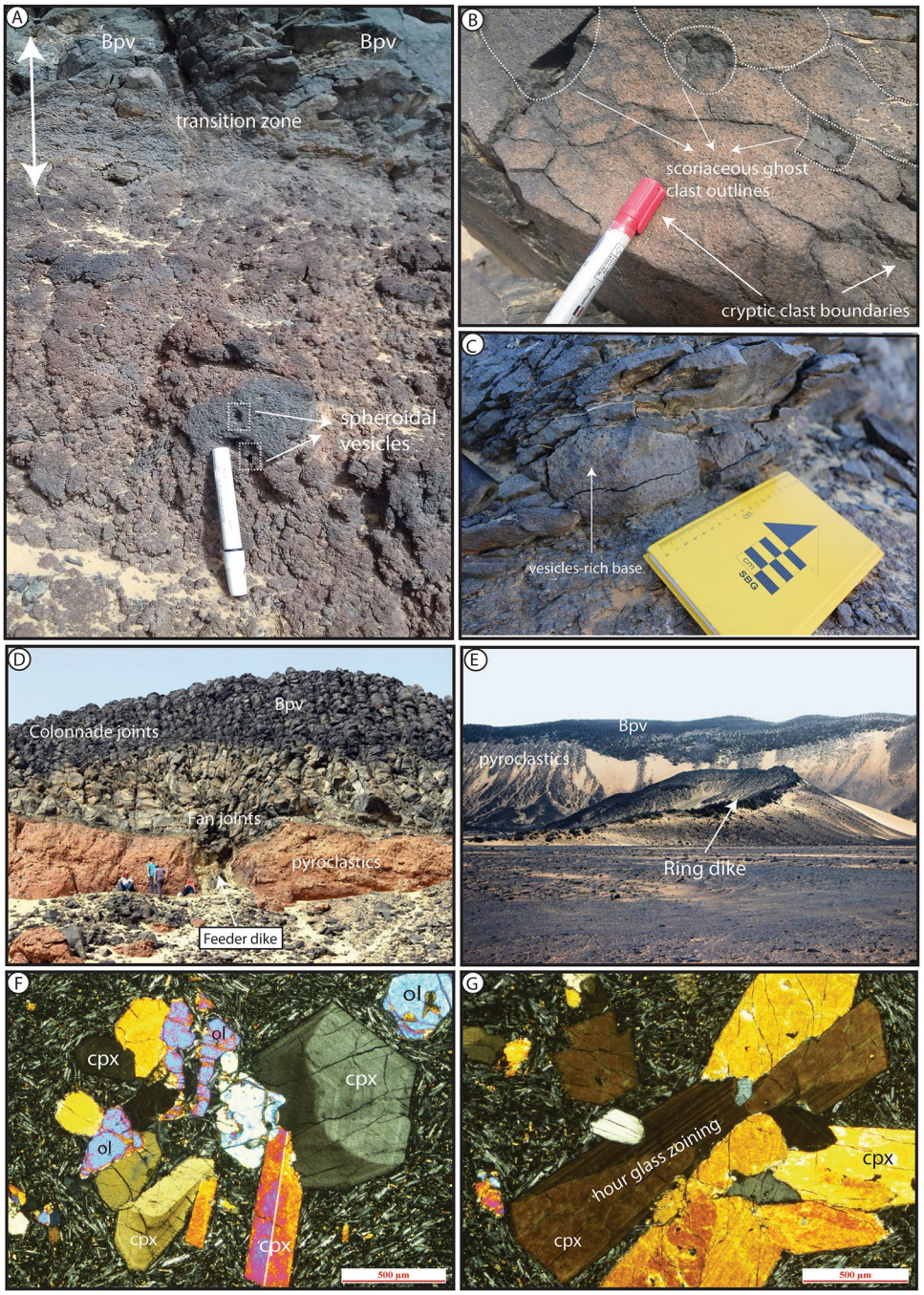

Fig. 6 **A** close-up view showing transition zone between underlying spatter-scoria beds (Unit3) and overlying vesicular porphyritic basalts of Pahoehoe flow (Bpv). Note the scorianeous nature with spherical-shaped vesicles of bomb-sized clasts. **B** Dispersed ghost scoriaceous clasts outlines in lower part of Bpv lavas, suggesting their original pyroclastic origin (Clastogenic lava flows). **C** Bpv Lava flows display spherical vesicles close to its base. Two joint tiers involving fan and colonnade joints characterize the Bpv lavas, unconformably overlying pyroclastic Unit 3. Note the prevailing of rounded pseudopillows and ball structure in the upper part of lava flows. Note vertical feeder dike cross cut the whole sequence. € Massive jointed ring dikes invade the Gabal Marssous sequence marking the final eruption phase. **F** Cross polarized light photomicrograph of coherent lava flows consisting rod-like olivine (ol) and subhedral-euhedral six-sided zoned clinopyroxene (cpx) set in plagioclase laths-rich matrix exhibiting fluidic texture. **G** Cross polarized light photomicrograph of Subhedral glomeroporphyritic clinopyroxenes (cpx) showing hour glass or sector zoing set in plagioclase laths-rich matrix

layers of a thinly stratified alternation of ungraded to normally graded fine lapilli tuff (fLT) and fine tuff (fT) beds with characteristically planar low angle cross and dune bedding structure (Fig. 7A, B). Tuff breccia layers showing inverse grading (Fig. 7B), prevail towards the upper parts of this sequence. Beds from Unit 1 are enriched in juvenile clasts ranging from ash to lapilli together with ballistic bombs ranging in size from 5 up to 10 cm in size (Fig. 7C). Ash and lapilli grain size of black-colored volcanic cognate lithic clasts are also observed. Bombs embedded in the tuff/lapilli tuff sequence are equant to sub-equant and often exhibit impact sags and bread-crusted external surface (Fig. 7C, B). Chilled margins of the bomb-sized clasts (Fig. 7D) are common. These juvenile clasts occur as angular to amoeboid grains with different shapes (skeletal/spindle to blocky) bounded by sharp fractures and have incipient to moderate vesicularity. The color of the former vary from black to brown as the result of palagonitic alteration for the latter color. The blocky juvenile pyroclastics vary in crystallinity from brown microlitic sideromelane (SM) to black

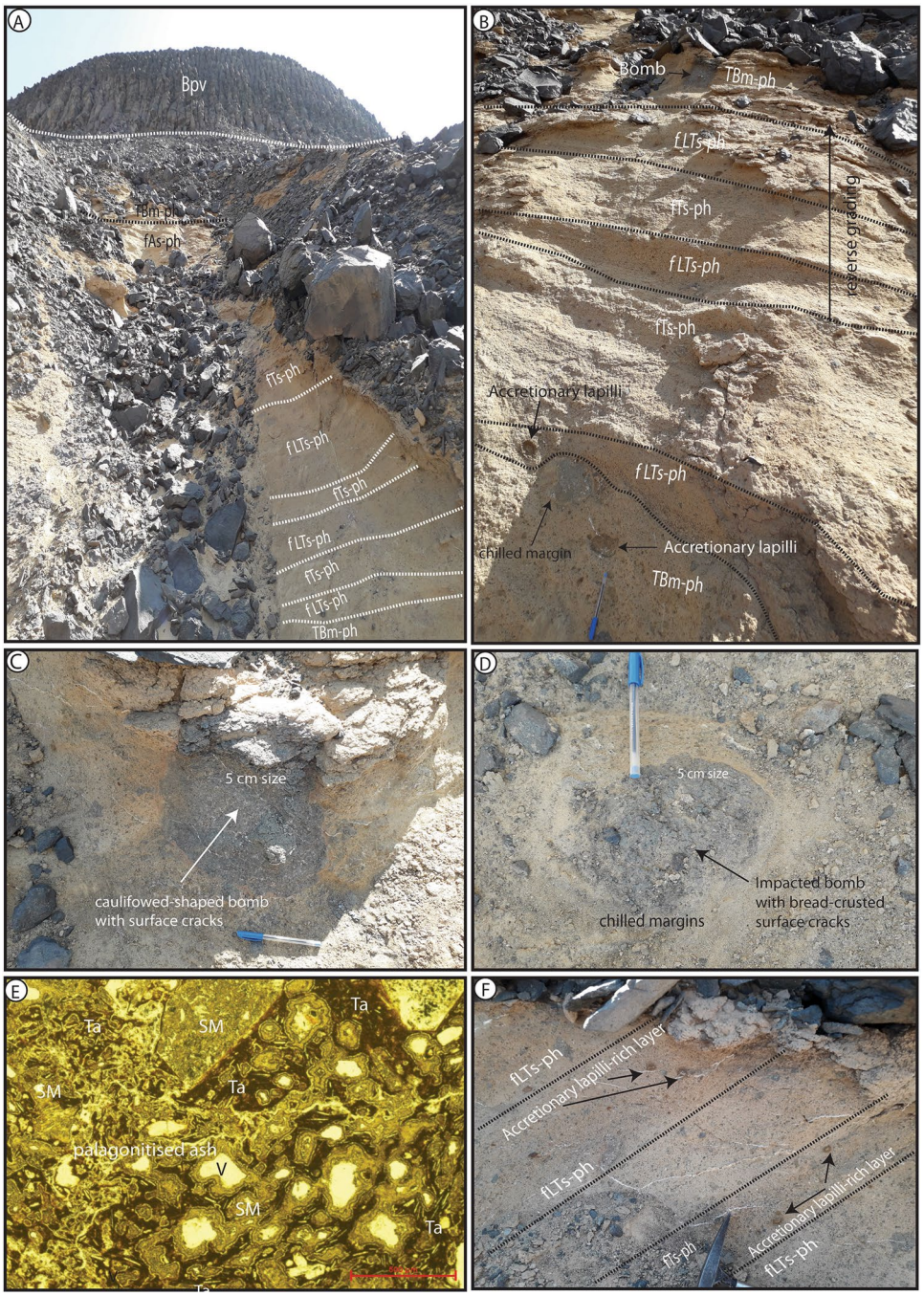

Fig. 7 **A** Pyroclastic Unit 1 (phreatomagmatic deposits) underlines the Bpv lavas along angular unconformity surface. Three lithofacies characterize pyroclastic unit 1 involving fLTs-Ph, phreatomagmatic fine lapilli tuffs; fTs-Ph, phreatomagmatic fine tuffs; TB-Ph, phreatomagmatic tuff breccia. **B** Close field view showing cross bedding and dune structures in fLTs-Ph/fTs-Ph/TB-Ph beds. **C** Cauliflower-shaped bomb with characteristically surface cracks. **D** Subrounded impacted bomb with bread-crusted surface cracks and chilled margins. **E** Plane polarized photomicrograph showing the dominance of blocky juvenile pyroclasts with low vesicularity and range of groundmass crystallinity from brown microlitic sideromelane (SM) to black tachylite (Ta). **F** Field photo showing three subfacies consisting of planar cross bedded fT-Ph and fLT-Ph that are enriched in micro-accretionary lapilli

tachylite (Ta) and occasionally are completely replaced by palagonite (Fig. 7E). Altered peridotite xenoliths are observed in the Unit 1. Accretionary lapilli are occasionally observed within tuff/lapilli tuff beds (Fig. 7F). These lapilli vary in shape from spherical to elongated form having 5 mm–2.5 cm in size, dispersed in palagonitized ashy matrix (Fig. 7B). The tuff's groundmass is aphanitic, holohyaline to hemicrystalline, consisting of olivine and pyroxene crystals, and fine tuff/lapilli-sized palagonized juvenile fragments together with black weathered clasts of lava flows. Fine-to medium-grained sandstone derived from the Bahariya Formation are observed in Unit 1 as ash-to lapilli-sized accessory lithic clasts.

Unit 2: lapilli tuff beds with bombs (LBb) *Description* In the eastern part of the scoria cone, Unit 2 underlies the lava flows (Fig. 4), but this unit is preserved below Unit 3 in its western part (Fig. 5). The rocks of this unit, ~20–40 m thick, are dark brown to red, poorly to moderately sorted, and clast-supported. This unit is composed of steeply inclined

nearly sub-vertical stack of beds, composing of decimeter- to meter-thick crudely stratified/bedded, medium to coarse lapilli tuff (mLTcb & cLTcb) grading to massive tuff breccia (TBm) (Fig. 8A–C). The base and topmost part of the sequence consist of moderately to well indurated, normally to reverse-graded thinly stratified alternation of medium to coarse lapilli beds fluctuating in thickness from < 1 to 5 cm (Fig. 8A, B). The layers of tuff breccias (~ 6 cm thick) occupy the middle stratigraphic part of this unit interbedded with lapilli-dominated beds along gradational borders (Fig. 8A). The latter are commonly planar non-erosional surfaces lacking any breaks with comparatively good lateral continuous dispersion up to many meters. In the field, juvenile fragments are subround to amoeboid glassy lapilli and ballistic bomb-sized clasts varying in shape from spongy, blocky, fluidal, spindle elongated or flattened (wood-shaped outlines) generated by plastic deformation (Fig. 8C–E). Bunch of moderately to highly coalesced/agglutinated, globular to elongated dense pyroclastic bombs with connected clast margins commonly merged together have been

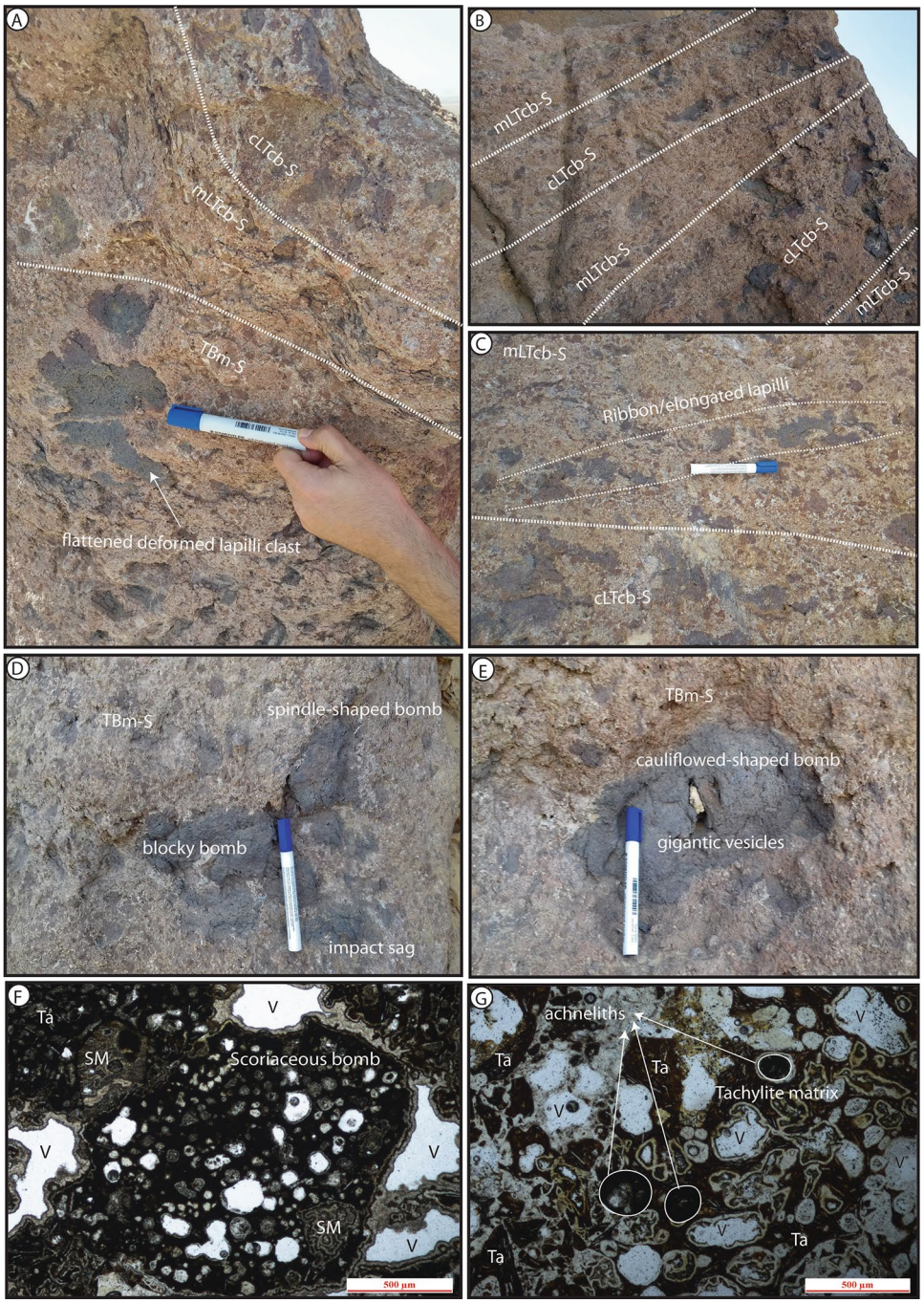

Fig. 8 **A** Pyroclastic Unit 2 (strombolian deposits) involve three lithofacies involving mLT-S, strombolian medium lapilli tuff; cLT-S, strombolian coarse lapilli tuff; TB-S, strombolian tuff breccia. Note flattened deformation and highly vesicularity of the juvenile clasts. **B** Crude bedding in deposits of Unit 2 marked by rhythmic alternating of mLT-S and cLT-S-rich layers. **C** Normal grading in mLT-and cLT-rich tephra displaying spindle, ribbon, and teardrop shape. **D** Close-up view of TB-S showing different morphology of bomb-sized clasts involving blocky- and spindle-shaped scoriaceous bomb-sized clasts with impact sag structure (**D**) and elongated cauliflowered-shaped bombs with gigantic vesicles and impact sag structure (**E**). **F** Plane polarized light photomicrograph demonstrating spherical vesicles of different size in scoriaceous bomb with large vugs set in sideromelane (SM) and tachyalite (Ta)-rich matrix. Note colloform texture of SM. **G** Plane polarized light photomicrograph showing globular shape of glass achneliths and abundant vugs set in tachyalite (Ta)-rich matrix

observed (Fig. 8D, E). Some of these flattened clasts are characterized by cauliflower shapes (Fig. 8D, E). Most of these coarse juvenile fragments are 4–15 cm in size with 18–20 cm in diameter in close packed clast-supported beds. The former occur as scattered lapilli/bombs at different stratigraphic height in the sequence. Ballistic bomb sags are noticed, displaying minor distortions (Fig. 8D, E). The exterior outline of juvenile clasts varies from even fluidal ropy surfaces (Fig. 8D) to scoriaceous spherical shape (Fig. 8F). The beds of this unit are characterized by high quantity of moderately to highly vesicular clasts (lapilli/bomb-rich materials) if compared to Unit 1. The vesicles are subrounded, spherical to elongation/stretched in shape (Figs. 8D–F), ranging in size from 2 to 50 mm and sometimes they are filled by calcite, zeolite, and brownish palagonite creating a colloform texture (Fig. 8F). Petrographically, the juvenile clasts are porphyritic rock with heterogeneous fabric, containing olivine, pyroxene, and Fe–Ti oxide that are dispersed in a holohyaline to hyalocrystalline black tachylite to microcrystalline yellowish sideromelane-rich matrix (Fig. 8F, G). Some blocky-type glassy fragments display < 1 mm rounded (Pele's tears) or ≤ 2 mm elongated, fluidal shaped clasts which may correspond to spheroidal droplet (achneliths) (Porritt et al. 2012; Carracedo-Sánchez et al. 2015). The achneliths are 50 µm–3 cm wide, massive, holohyaline, and comprise microliths set in tachylitic groundmass containing feldspar laths (Fig. 8G).

Unit 3: spatter-scoria bomb beds (Bb) *Description* Spatter and scoria bomb beds are well exposed at the western side of the scoria cone, unconformably overlying the Unit 2 along sharp contact (Figs. 5, 9A). Their upper boundary is transitional interfingering with the overlying lava flows (Fig. 6A). These beds are extremely juvenile-rich, internally massive, black to dark red in color, moderately to well sorted, clast-supported lacking any internal bedding. They are intensely oxidized to redish colour near the feeder dike (Fig. 6D). Spatter and scoria deposits include moderately to highly welded coarse lapilli tuff (cLT) grading to agglomerate (BA) with thickness up to 5 m (Fig. 9B, C). They often exhibit agglutination and their juvenile clasts have an obviously high vesicularity, demonstrating scoriaceous framework. The beds of Unit 3 have fragments varying in size from coarse lapilli to blocks and bombs which are better sorted than those in Unit 2. The spatter deposits comprise moderate welded very dense to dense spatters (medium/coarse lapilli tuff) at the base and highly welded varieties (bombs-rich vuggy spatter) grading to lava flows at the top section (Fig. 9D, E) as previously projected by Carracedo-Sánchez et al. (2012) for the lithofacies classification. The protrusions of these rocks consist of rhythmic alternating spheroidal scoriaceous lapilli- and ballistic bomb-sized clasts with blocks (Fig. 9B–G). In some locations, the bomb-sized clasts forming agglomerate (BA) occur at the base followed by thick horizons of coarse lapilli-sized beds (Fig. 10A). The average clast size varies from 5 to 10 cm and some fragments occasionally attain a size of 5 × 20 cm. The juvenile bombs display different forms and shapes varying subequant, elongate, spindle, or bulbous clasts with bread-crusted cauliflower and/or ropy surface/or rheomorphic textures that are locally stacked or bunched clasts set in a fine-grained clastic matrix (Fig. 9B–H/10A, B). Folded- and convolute outlines with flow-banding interiors characterizing the bomb clasts together with typically agglutination and/or coalescence have been observed (Fig. 9G, H, 10A, B). Some accidental basaltic clasts (5 cm in length) has been detected within these deposits (Fig. 10C, D). Most of the spheroidal bombs/lapilli and Ash-size clasts are highly welded and composite (Fig. 10B) (Carracedo Sánchez et al. 2009, 2010) with abundant voids or hollows in their interiors that are recorded within the spatter deposits. Ash-size spheroidal clasts resemble to crystals/spinning droplets, achnoliths, or pelletal lapilli (Junqueira-Brod et al. 1999; Alvarado et al. 2011; Carracedo-Sánchez et al. 2015). The composite bombs are composed of ash- to lapilli-size welded clasts enclosed in a cryptocrystalline groundmass (Fig. 10D). These clasts involve mantle xenoliths comprising olivine and pyroxene, juvenile/crystals fragments, spinning/isotropic droplets, and achnoliths or melt blobs (Fig. 10E). They are microcrystalline, showing hyalocrystalline texture with microlitic matrix and highly vesicular tachylitic mesostasis. The matrix involves curved, ill-defined cryptocrystalline carapaces consisting of quenched juvenile microphenocrysts and tachylitic microlites with hollows. The latter are subrounded and irregular in shape, ranging from 2 mm to 5 mm in size and filled by calcite, acicular zeolite, and brownish palagonite (Fig.10F).

Coherent subvolcanic intrusions *Description* The intrusions appear in various forms and have variation in thickness (0.5–3 m) with lengths from 5 to ~ 100 m (Fig. 6E). They occur as curved subvertical to vertical coherent igneous rock bodies.The former strike NE and NW-trend displaying ring outcrops and dips 35° to the northeast that are recorded at the southern parts of the scoria cone (Fig. 6E). They display variation in thickness restricted between 3 m at the base and 20 m thick at the dike head with 100 m length, establishing segmented dikes (Fig. 6E). The latter has been detected along the base of the pahoehoe lava flows (Bpv) and the underlying pyroclastic deposits (Fig. 6D) forming a funnel-like zone with localized extensive thermal alterations adjacent to dike and near the contact between lava flow and pyroclastic rock with amoeboid borders (Fig. 6D).These coherent lava dikes are aphanitic, massive, black in color, poorly vesicular, and coherent basalt consisting of olivine and clinopyroxene set in

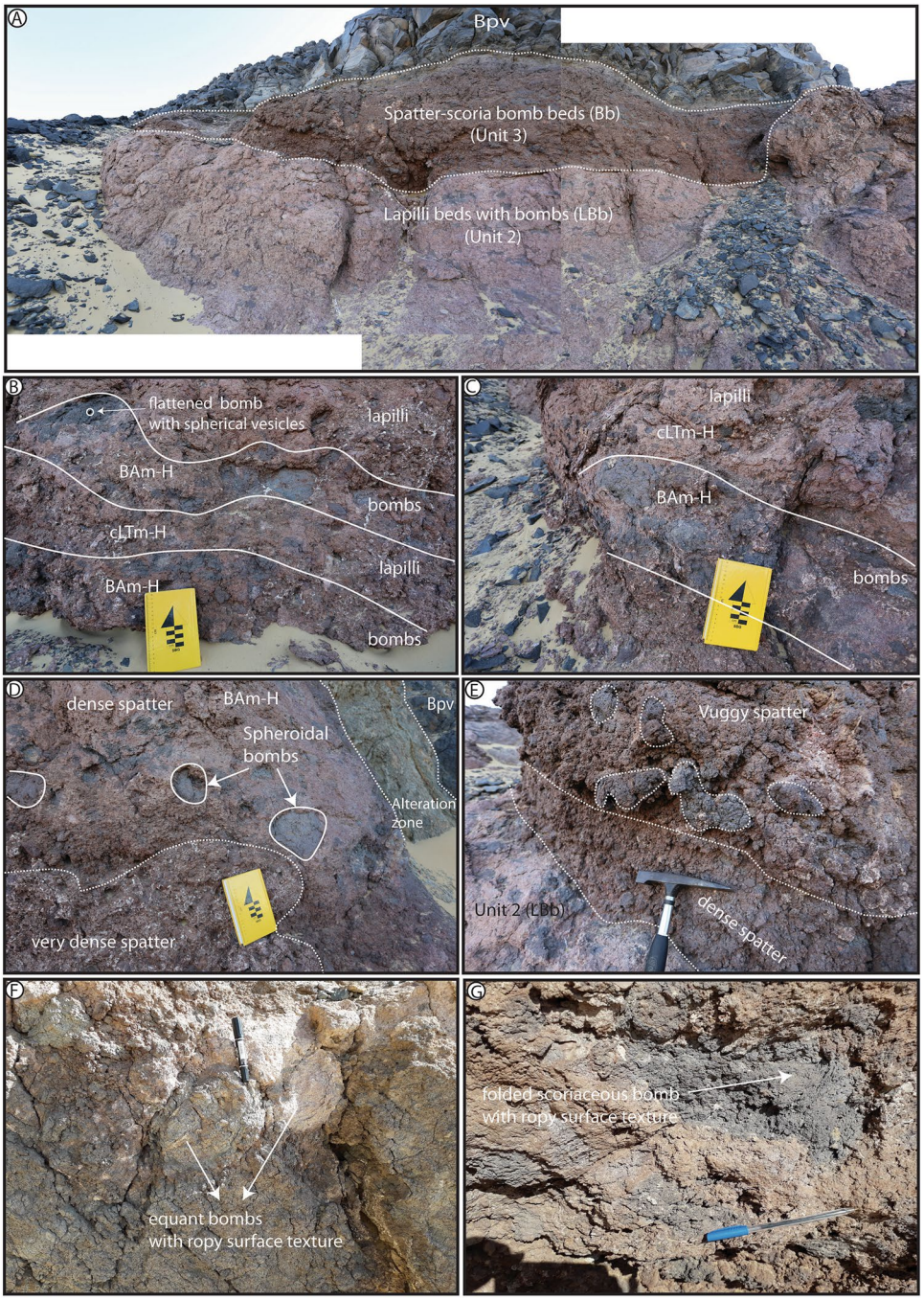

Fig. 9 **A** Viewpoint of the western sector of the Marssous cone showing spatter-scoria beds (Bb) and overlying clastogenetic lava flows (Bpv) forming Unit 3 that underlies strombolian lapilli-bomb tephra (Unit 2). Two lithofacies characterize pyroclastic Unit 3 involving cLTm-H, Hawaiin coarse massive lapillituff; BAm-H, Hawaiin massive bomb agglomerate. **B** Massive spatter deposit mainly marked by differences in clast sizes (bomb-rich vs. lapillirich levels). **C** Thick lenses of broken and breadcrusted clast-supported bomb-sized tephra (BA) alternating with lapilli-sized tephra (cLT). **D** Close-up view of Bb beds showing variation in rock compactness from very dense to dense spatter deposits. Note spheroidal lapilli/bomb tephra passing to transitional alteration zone separating spatters and clastogenic lava flows (Bpv). **E** Detail of the progressive densification (from top to bottom) from dense to vuggy spatter deposits of Hawaiian style. Clast outlines and the interclasts hollows disappear gradually with the increase of the clast coalescence. **F** Close-up of BAm showing equant bombs with ropy surface textures and convolute concentric fabric. **G** Elongate deformed bombs with ropy surface texture and cauliflower morphology

aphyric matrix. In addition, pyroclastic dikes have been observed which cross cut the pyroclastic Unit 2 (LBb). These clastic dikes are aligned along NW-SE and consist of lapilli/block fragments and brown to black juvenile clasts within a phanitic fine-grained matrix, analogous to those of the LBb rocks (Fig. 10G). They vary in thickness from 10 cm to 2 m and in length from 3 to 5 m (Fig. 12G).

SEM investigation

The SEM studies (Fig. 11) display that the exposed pyroclastic deposits at Gabal Marssous further support diverse modes of fragmentation (phreatomagmatic vs. magmatic eruptive style) based on their miscellaneous morphologies of juvenile pyroclasts (Heiken 1974; Honnorez and Kirst

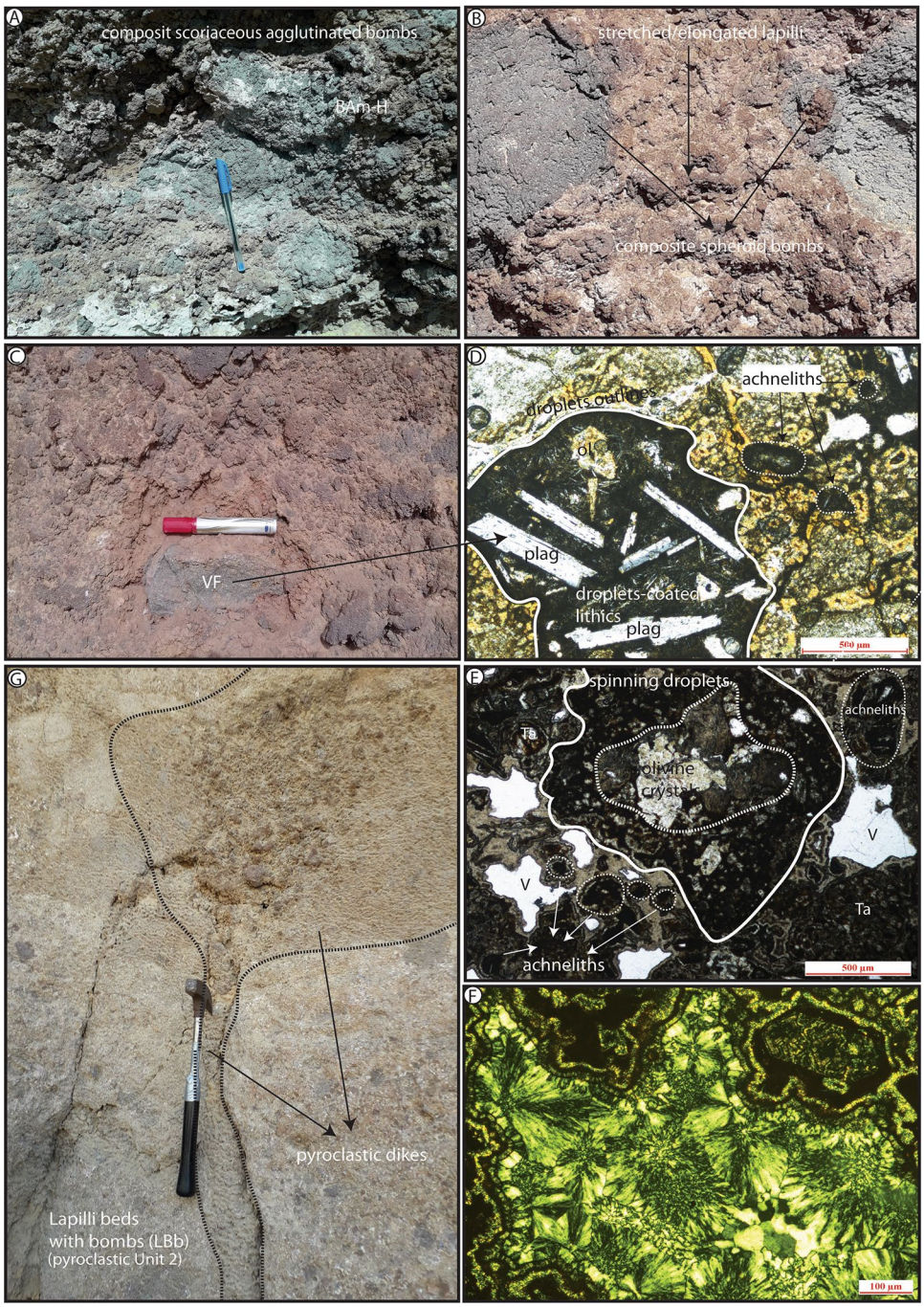

Fig. 10 **A** Highly welded spatter with deformed, subvertical, ropy fabric. **B** Scoriaceous Composite spheroid bombs with cauliflower morphology. Note deformed lapilli-sized juvenile clast with ropy surface texture. **C** Aphyric basaltic fragment is observed within the spatter deposits. **D** Plane polarized photomicrograph showing petrographic composition of basaltic fragments consisting of olivine (ol) and plagioclase (plag) set in tachylitic matrix. Note rounded glass sphers known as achneliths. **E** plane polarized photomicrograph of composite spheroidal bomb consisting of olivine crystals-rich core (Iherzolite xenolith ?) surrounded by spinning droplet with diffuse contours. Note the presence of cryptodroplets of achneliths together with abundant vesicles set in cryptocrystalline tachylitic (Ta) matrix. **F** Cross polarized light photomicrograph showing Gel Globules of palagonite totally replace juvenile clasts (extensive palagonization) coupled with the formation of secondary minerals (mainly acicular zeolites, calcite and clay). **G** Massive vertical pyroclastic dikes crosscut the pyroclastic Unit 2, marking the final eruption phase. Note the thickness variation from thin at the base to thick at the dike head, demonstrating dike segmentation

1975; Wohletz and Sheridan 1983; Wohletz 1986; Heiken and Wohletz 1991).

Unit 1 is made of juvenile, crystal, and lithic clasts ranging from ash to lapilli-sized pyroclasts. Unit 1 is dominated by the presence of unequant, blocky and glassy shards (Figs.11A-C). Curved fractures and perlitic cracks characterize these juvenile clasts displaying spongy appearance (Fig.11A). Clast exteriors can be planar but commonly are even (Fig. 11A, C). Its shape displays irregular, subangular, and spherical masses forming moss-like morphology (Fig. 11A, C), as an indication of fine ash derived from explosive phreatomagmatic fragmentation (Heiken and Wohletz 1991). Juvenile pyroclasts from Unit 1 has low vesicularity having globular vesicles (Fig. 11E). The products of Unit 1 exhibit an intense alteration involving zeolite-filling cavities and palagonization (Fig. 11B–E), which reveal the attendance of a hydrous phase in this unit. Such alteration covers elongate juvenile and crystal clasts (Fig. 11B, D).

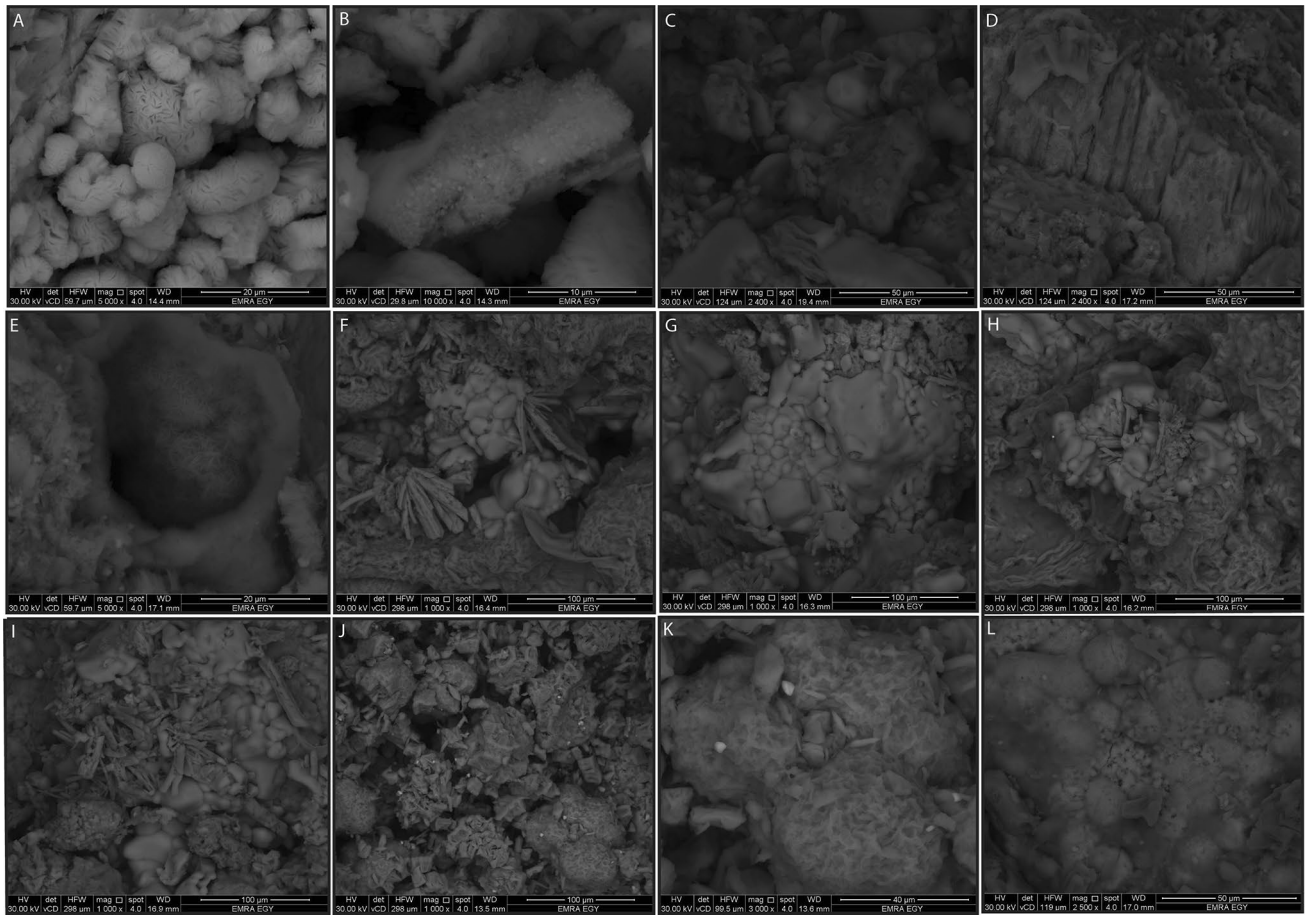

Fig. 11 SEM images for pyroclastics belonging to phreatomagmatic (**A–E**), strombolian (**F–H**), and Hawaiian phase (**I–L**). **A** Juvenile clasts are characterized by planar surface with curved fractures and perlitic cracks displaying spongy appearance. Cracks may form by mechanical or chemical processes and are probably a result of volume changes during hydration, typical of phreatomagmatic eruptions (Clarke et al. 2009). **B** Secondary alteration coating on glass shard. **C** Ash to tuff-sized tephra exhibits unequant, a highly irregular surface consisting of small globular and angular masses blocky particles forming moss-like morphology. This shape also is characteristic of fine grained pyroclasts of phreatomagmatic origin (Heiken and Wohletz 1991). **D** Phenocrysts partly coated with altered basaltic glass shards. **E** Dish-shaped morphology with localised acicular zeolite growth and secondary alteration coating on pyroclastic clasts. **F** Moderately sorted, spheroidal shape and moderate to high vesicularity together with coalescence aggregates characterize strombolian compared with early phreatomagmatic pyroclastics. **G** Composite lapilli-sized tephra consist of cored crystal fragments (most properly pyroxene) and globular isotropic glass droplets. **H** Various pyroclastics involving globular glass clasts (i.e., achneliths), droplet-coated crystals, and scoriaceous glass fragments typify the strombolian eruption of unit 2. **I** Variable size of achneliths Coalescence (i.e., melt blobs) exhibit botryoidal aggregates. **J** Spinning droplet with diffuse contours and a core made of crystal droplets surrounded by botryoidal glass globules and oriented isotropic droplets forming composite spheroidal lapilli/bombs. Note spiral arrangement of glass constituents. **K** Coalescence of glass globules with secondary palagonite and zeolite-filling voids or hollows between the globules. **L** Highly vesicular scoriaceous juvenile fragments with spherical and deformed (flattened) shape of some of the vesicles.SEM exhibits the fresh surface looking of the most of juvenile clasts in Unit 2 and Unit 3 compared with this in Unit 1

In Unit 2, juvenile clasts are highly scoriaceous and less blocky if compared with Unit 1 (Fig. 11F–H). SEM images show that Unit 2 comprises coalescence aggregates of cored crystal clasts (mostly pyroxene) and globular isotropic glass droplets confirming composite lapilli-sized textures (Fig. 11G–H). Less amount of juvenile pyroclasts with moss-like morphology were still noted compared with Unit 1. Vesicles in juvenile clasts are rounded to elongated in shape, which are frequently significantly larger (> 100 µm) (Fig. 11H) compared with this in Unit 1. More asymmetrical shapes are due to the sporadic coalescence of glass bubbles.

In Unit 3, the largest proportion of the fragments having variable size (lapilli to bomb) are composed of spheroical composite bombs, similar to those im Calatrava volcanic field, Spain (Carracedo Sánchez et al. 2009). The amalgamation of these fragments deliberates a botryoidal or cauliflower-like facet (Fig. 11I, J). Spinning droplets show micro-concentric folded layers (Fig.11J), infrequently in spiral arrangement and the predominant components of glass

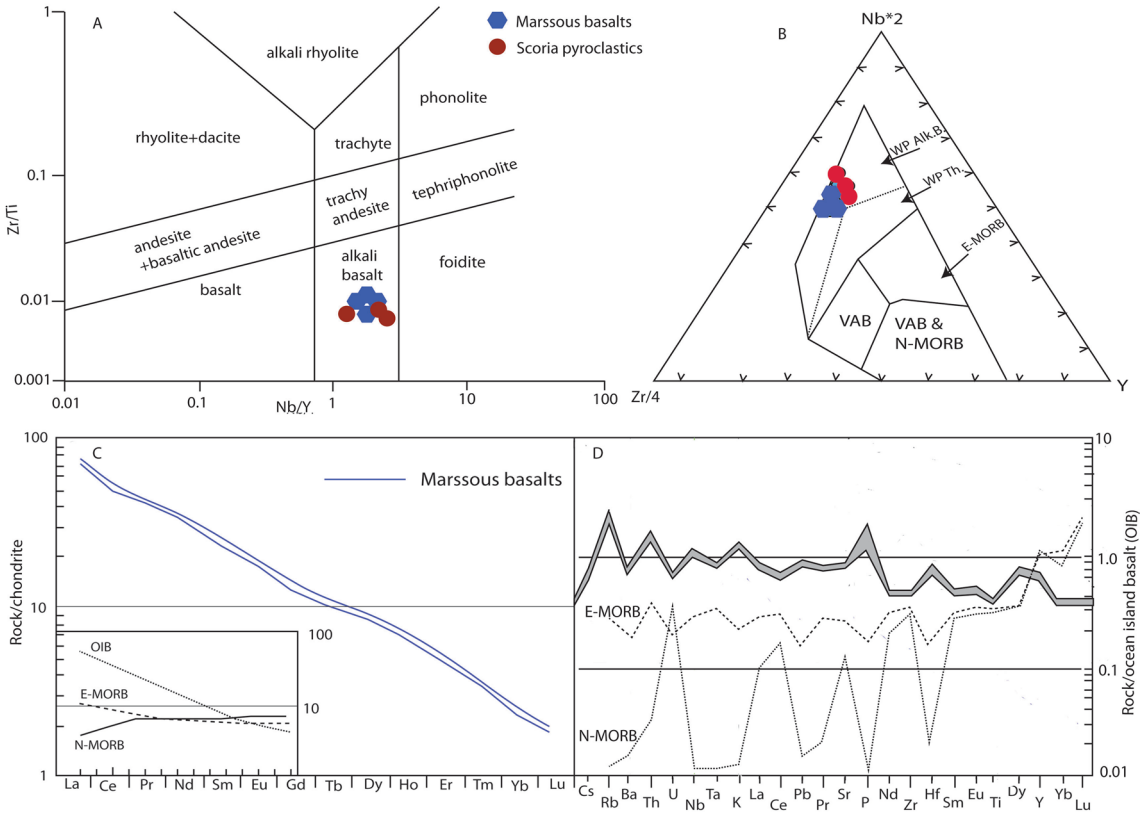

Fig. 12 Geochemical characteristics of the pyroclastics and lava flows. **A** Zr/Ti vs. Nb/Y diagram (after Winchester and Floyd 1976). **B** Zr/4–Y–2Nb discrimination diagram (Meschede 1986). *WP* within plate, *Alk B* alkali basalt, *ThB* tholeiitic basalt, E-*MORB* enriched Mid Ocean Ridge Basalt, *N-MORB* Normal Mid Ocean Ridge Basalt. **C** Chondrite normalized rare earth element for lava flows. **D** Ocean island basalt (OIB) normalized major/trace elements for lava flows The averages of N- and E-type MORB and oceanic island basalts (OIB) are involved for comparison (after Sun and McDonough 1989)

spherules/globules (Fig. 11K). The incorporation of such globules is equivalent and comparable to what so called spherical lava spray (i.e., "melt blobs" or "achneliths") (e.g., Walker and Croasdale 1971). Most of the juvenile pyroclasts reveal high degree of coalescence (Fig. 11G–K). They are completely lacking in Unit 1. The juvenile particles have large hollows and exhibit different strengths of palagonitization and fragmentation (Fig. 11K), though negligible in extent compared with this in Unit 1. The fresh surface looking of the juvenile glass clasts (Fig. 11) is an indicative of low magnitude of palagonitisation and degree of hydrous alteration in Unit 3. Juvenile clasts (Fig. 11L) is characterized by abundant number of oval to spherical vesicles with respect to those of Units 1 and 2.

Geochemistry

The Marssous's basalts are characterized by low loss on ignition (LOI, < 2 wt%), however the scoria samples show high LOI (4–10) and total alkali, suggesting the probable mobilization of elements such as K, Rb, Ba, and Sr. The mobilization of the latter elements is due to the alterations and glass decomposition accompanying the deposition of clays and zeolites in vesicles characterizing the scoria samples. This leads to an enhancement of alkali interdiffusion through glass hydration (Johnson and Smellie 2007). The chemical composition of the basaltic and scoria samples is similar in some major (TiO_2, P_2O_5) and trace elements (e.g., Ni, Cr, Th, Y, Zr, Nb) confirming their genetic link and derivation from the same parental magma, independently of magma fragmentation.

We base our geochemical interpretations on the immobile elements that return the original nature of the lavas prior to alteration, using the Nb/Y vs. Zr/Ti binary diagram of Winchester and Floyd (1976), modified by Pearce (1996). On this diagram (Fig. 12A), the basaltic and scoria samples plot within the alkali basalt field.Tectonic discrimination ternary diagram (Fig. 12B) that relys on immobile elements approves the geochemical characteristics of the within plate alkali basalts. In chondrite-normalized REE plots (normalization values are those of McDonough and Sun 1995) (Fig. 12C), all coherent lavas contain high LREE contents if compared with HREE [$(La/Yb)_N$ ~21, $Tb/Lu)_N$ = 2.54, Nb/Yb ratio =36] that are indicative of derivation from an

enriched mantle source.The high ratios of Zr/Hf (47) , La/Nb (0.57) and Ba/Nb (7.30) for the basalts suggest their derivations from asthenosphere mantle (Taylor and McLennan 1985). In ocean island basalt (OIB)-normalized plot (Fig. 12D), the Marssous basalts has a pattern that slightly resembles the OIB pattern, but high Rb and P together with relatively low some incompatible trace and REE characterize the Marssous basalts relative to OIB. This can further be supported by the similarities of Nb/Ta, Nb/U and Ce/Pb ratios in both the OIB (e.g., Nb/Ta =17.5, Nb/U = 47, Ce/Pb = 25 ± 5) (Hofmann 2003) and the studied basalts (23, 44 and 28, respectively). The basalts have low Th/La (0.12–0.13) and Th/Ce (0.05–0.06) ratios, which rule out the possibility of significant crustal contamination through their eruptions to the surface (Sun and McDonough 1989).

Discussion

Facies architecture and eruptive mechanism

Marssous's scoria cone can be deliberated a unique composite volcano in light of eruptive fragmentations having different eruptive dynamisms that prevailed during the diverse eruptive styles. The field, sedimentological, petrographical, and SEM features of the pyroclastic deposits demonstrated great variations in their lithofacies, grain size, shape, degree of vesiculations, and surface morphology which reflect synchronous and evolutionary multistages of nucleation and growth (Fig. 11). The preserved Marssous's succession represents an eroded maar/tuff ring with intra-crater scoria cone, as supported by: (i) there is a well-localized, semicircular volcanic depression (Fig. 1E), (ii) the rock outcrops have crescent edifice, (iii) the scoria's bowl is filled with lava flows, ash beds (Ab), lapillituff beds with bombs (LBb), and scorianeous bomb agglomerates (BA), representing vent to crater zone. The absence of prevailing paloesoils and erosive surfaces in the volcanic sequences suggests that these sequences are closely related in time belonging to the same eruption and emplaced consecutively, similar to monogenetic volcanoes elsewhere (e.g., Lorenz 1986; Németh et al. 2003b).

The development of the Miocene succession in the rift-related Marssous basin forming scoria cone can be shortened in six successive phases (Fig. 13) formed by asthenospheric mantle-derived magmas to the surface without any significant crustal contamination as mentioned by Khalaf and Sano (2020). These phases comprise magmatic pahoehoe effusive (Bpm) and magmatic explosive phases involving phreatomagmatic (Unit 1), Strombolian (Unit 2), and Hawaiian (Unit 3) explosive eruptions together with pahoehoe lava flow (Bpv) and subvolcanic intrusions. The fluctuation of lava flows and pyroclastic rocks in the stratigraphic list (Figs. 4, 5) gives evidence for time overlapping, signifying diverse modes of fragmentation and dissimilar eruptive processes. The variations in the effusive and magmatic explosive styles may be accredited to oscillations in magma flow circumstances linked to changes in crystallinity and vesicularity of the injected magma (Cimarelli et al. 2010; Sable et al. 2006; Saucedo et al. 2017). These eruptive variations inferred to form in distinct eruptive phases but still within a narrow time frame attesting the fundamentally monogenetic behaviour of the seemingly complex volcano (White 1990; Németh and Kereszturi 2015; Smith and Nemeth 2017).

Phase 1: Pahoehoe lava flow (Bpm)

The early phase in the Marssous area began by the eruption of the basalts (Bpm) of pahoehoe type, superimposing the Bahariya Formation of Upper Cretaceous. The massive characters and convolute surfaces of the basalts (Bpm) typify a pahoehoe lava flow (Rowland and Walker 1987; Self et al. 1998). A low-slopes and low effusion rates facilitate the development of pahoehoe flows (Rowland and Walker 1987; Belousov and Belousova 2018). The horizontal columns characterizing Bpm lava indicate vertical cooling front and a strong limited deflection of isotherms as the effect of meteoric water appearance during lava eruption (Long and Wood 1986; Sheth et al. 2015). These basaltic lavas typically issue from the cone base as a fissure eruption in the form of either coherent flows or overflow/or breaking of a lava lake from small fractures, similar to the mafic monogenetic volcanoes elsewhere (Thordarson and Self 1993; Keating et al. 2008; Valentine and Gregg 2008; Lefebvre et al. 2012, 2016). The homogenous texture of these flows reflect rapid magma ascent and flow emplacement, implying lack of lava stagnation and short residence time in crustal reservoirs as the result of continuous lava supply (Hon et al. 1994; Cashman et al. 2014), analogous to Hawaii and other subaerial volcanoes worldwide (e.g., Belousov and Belousova 2018). The time break between the eruption of Miocene lavas and accumulation of the sediments of the Bahariya Formation was long enough to create distinct topographic that captured the outpouring lava.

Phase 2: phreatomagmatic explosive phase

The second phase of the volcano growth started by the vent-opening eruption of pyroclastic unit 1 typical for explosive phreatomagmatic eruptions that exhumed an explosion crater in the Upper Cretaceous substrate. It was triggered by the intersection of the rising magma with the aquifer of the Bahariya Formation, as evidenced by the presence of quartz/feldspar lithic clasts. The occurrence of the latter reflect excavation into the country rock and fragmentation likely occurred at shallow depth, producing vertical mingling of

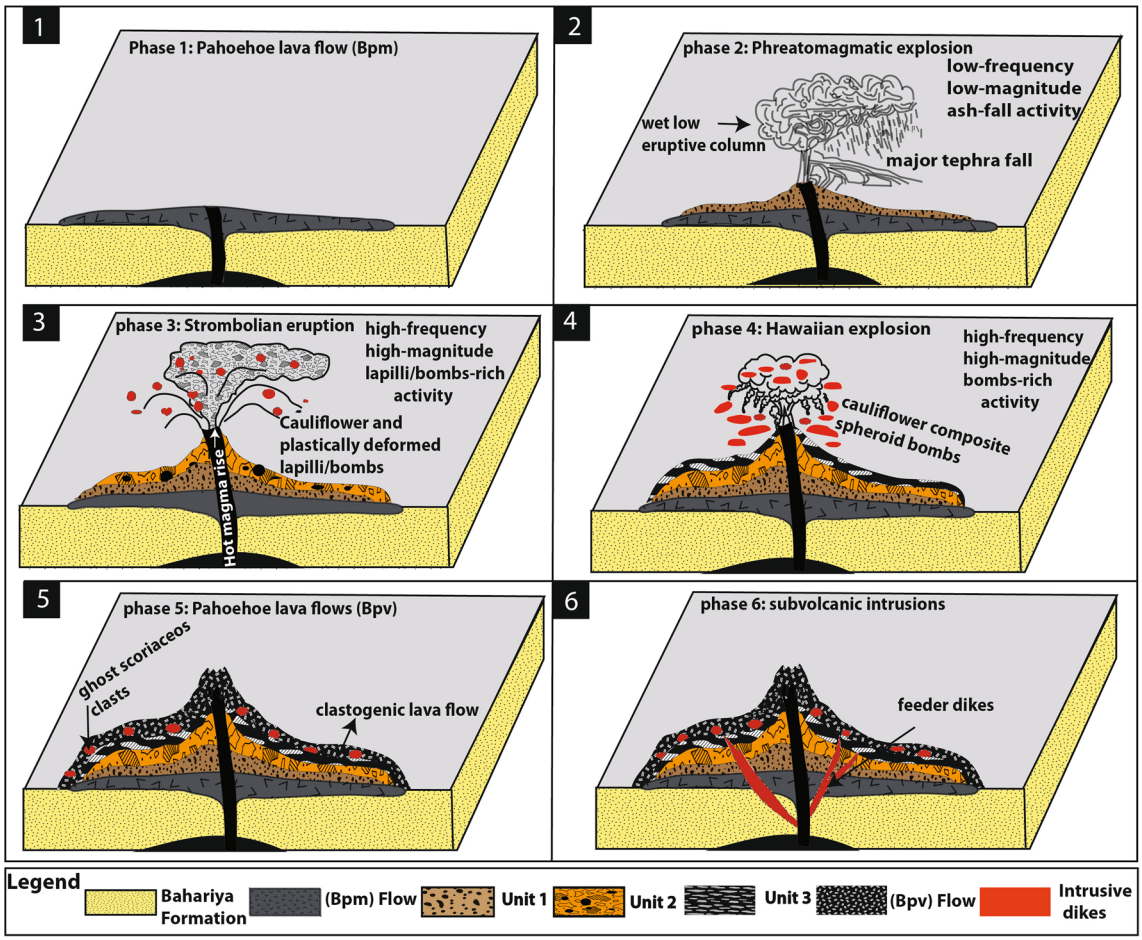

Fig. 13 Cartoon sketch of inferred eruptive processes, displaying six consecutive evolutionary phases of El Marssous scoria cone. **Phase 1** Lava effusion commences and issues from the cone base either as coherent lava flows or breaking of lava pond inside the scoria cone through small fractures. **Phase 2** Phreatomagmatic eruption starts when groundwater-rich Bahariya Fm, aquifer is interrupted by rising magma. Phase 3. Reduced magma–water interaction leads to strombolian eruptive style and development of cauliflower and plastic deformed lapilli-bomb-rich tephra. **Phase 4** Eruption progresses to a purely Hawaiin regime, lacking evidence for the involvement of external water: explosive fragmentation, fluidized transport, and agglutination/coalescence of pyroclasts in the gas thrust region of the eruption column (gas-rich phase) lead to formation of flattened and spheroidal composite lapilli- to bomb-sized tephra. **Phase 5** Eruption of Pahoehoe lava flows with characteristically ghost soriaceous clasts localized along spatter-lava flows forming clastogenic flows. **Phase 6** In the final eruptive history of scoria cone, injection of squeezed lava/tephra through fractures produce coherent and pyroclastic dikes that fed the pyroclastics and lava flows

magma-derived juvenile debris and country rocks as the result of downward subsidence during the eruption (White and Ross 2011; Valentine and White 2012). The rocks of this phase are paler in colour, poorly sorted, bedded, fLTs-ph to fTs-ph grading to TBm-ph (Fig. 7) having a high quantity of fine matrix (i.e., matrix-supported). The morphological and textural features of the juvenile clasts (angular blocky clasts with surface particle adherings, fine grain size, poor sorting, low amount of vesicles, alteration mineral growths, palagonitization, etc) deliver evidence on the mode of magma fragmentation, as consequence of phreatomagmatic explosions (Heiken 1972; Wohletz and SHeridan 1983; Lorenz 1985, 1987; White 1991a, b; Houghton et al. 1996; Zimanowski et al. 1997; Buettner et al. 2002; Rosi et al. 2006; Latutrie and Ross 2018; Ross et al. 2018; Németh and Kósik 2020). The latter interpretation is reinforced by the sedimentary characteristics (planar, low angle cross bedding and dune, good grading, fine-grained size) of the pervasive lithofacies fLT and fT which reflect deposition by lateral moving flows forming low-energy, wet pyroclastic surges of the pyroclastic density currents (PDCs) and not from pyroclast fallout (Fisher and Waters 1970; Schumacher and Schmincke 1991; Sumner and Branney 2002). The architecture of these bedded deposits comprises millimetric to centimeters subvertical beds (Fig. 7B) designed by several deep explosions triggering surges ejection (e.g.,Bélanger and Ross 2018; Latutrie and Ross 2019). Moreover, the occurrence of accretionary lapilli and impact sags also give a mark of explosive

magma-water interaction forming phreatomagmatic mafic tephra (Wohletz and Sheridan 1983; Johnson 1989; Chough and Sohn 1990; Sohn and Chough 1990; Cioni et al 1992; Lorenz 2000; Németh et al. 2001; Sottili et al. 2010; Lefebvre 2013; Brand et al. 2014; Murcia et al., 2015; Németh and Kósik 2020; Ureta et al. 2020a, b).

The shift from Phase 1 (effusion-dominated) to Phase 2 (phreatomagmatic explosion-dominated) suggests a major modification in the eruptive mechanism as the result of rapid fluctuations in magma discharge, volatile flux, and ground water flow variations to switch magmatic effusive eruptions to explosive phases. This shift can take place due to a decline in the discharge rate, permitting link between magma and water in the early eruptive initial stage (Houghton et al. 1999). The great proportion of fine particles (ash & fine lapilli) within Unit 1 is good evidence for the increased efficiency of the fragmentation and fast decompression rates without any major magma storage as the magma approaching the surface expands (Walker 1973) during phreatomagmatic phase (Houghton and Smith 1993; Buettner et al. 2002; Zimanowski and Buettner 2003; González et al. 2019; Murcia and Németh 2020; Ureta et al. 2021). Documentation of phreatomagmatism in the study area proposes widespread groundwater accessibility (e.g., Sohn 1996; Kereszturi et al. 2012), highlighting the function of the substrate hydrogeological circumstances in the growth of the phreatomagmatic eruptive phase.

Phase 3: strombolian explosive phase

Phase 3 returns a rapid switch from phreatomagmatic to a Strombolian Phase that produced structureless to diffusely bedded, and moderate sorted pyroclastic deposits consisting of medium-to coarse lapilli tuffs (mLTcb-S to cLTcb-S) interbedded with massive tuff breccias, (TBm-S on Fig. 8) that hinder size grading, forming magmatic explosive rocks which overlain the previous deposits. Unit 2 is inferred as ballistics and air fallout deposit that rises in the highest part of an eruptive column as scoriaceous expelled juvenile tephra mixed with gas bubbles and fluid clots on ballistic trajectories together with recycled blocks (Fisher and Schmincke 1984; Cas and Wright 1987; Martin and Nemeth 2005). Pyroclastic deposits of Unit 2 are dominated by coarse-grained juvenile clasts (lapilli/bomb) with moderate to high vesiculation, small portion of fine ash, and lack of matrix (clast-supported) that typifies pyroclastic facies of Strombolian eruptions via less energetic explosions compared to wet surge deposit of Unit 2 comprising fine-grained Tb lithofacies (McGetchin et al. 1974; Houghton and Hackett 1984; Martin and Nemeth 2006; Rowland et al. 2009; Gurioli et al. 2014).

Strombolian eruptions have flattening and agglutinated clasts (Fig. 8A–C) which infer load compaction upon landing and sporadically higher retained heat that were formed as separate eruptions because of the gas decoupling (Houghton and Gonnermann 2008). Stretched vesicles recorded in juvenile bomb clasts may occur either during transport (e.g., fluidal bombs), or shearing near the conduit boundaries during magma ascent, demonstrating degassing procedures and post depositional vesiculation in magma (Branney and Kokelaar 1992; Polacci et al. 2003). The fall deposit can be inferred as eruptive pulses with a high ascent rate, viscosity, and magma ascent velocity. All these influences facilitate accretion and sporadic Strombolian overflowing of gas pockets at shallow depth because the high gas bubbles outbursts enable substantial coalescence when the magma rise is comparatively quick with decline effect of external water inflow (Parfitt and Wilson 1995; Vergniolle and Mangan 2000; Parfitt 2004; Ureta et al. 2021). Volatile exsolution and decompressional expansion have great effect on bubble coalescence processes (Fig. 11) (Cashman et al. 2014; Shea et al., 2010; Murtagh and White 2013). The change to a Strombolian style happens when a restricted water supply (ponded lake?) became exhausted or if the water supply was condensed as the consequence of cyclical variations (Lorenz 1986; Parfitt 2004; Kosik et al. 2016).

Phase 4: Hawaiian explosive phase

This eruption phase unconformable overlying Unit 2, represents the fourth explosive phase of the Marssous scoria cone (Fig. 13). The former corresponds to a clast-supported, massive, scoriaceous to agglutinated scoria and spatter clasts (cLTm-H to BAm-H on Fig. 9). Coarsening-upward of spatter deposits suggest that this phase was characterized by a moderately, explosive activity gradually increasing in energy aided by an increase in the mass magma discharge and magma ascent speed (Parfitt and Wilson 1995; Parfitt 2004; Andronico et al. 2008; Valentine and Gregg 2008). The transition from lapillituff-bombs (LBb) to spatter-scoria (Bb) fall deposit suggests a change of the eruptive style from Strombolian to Hawaiin (Parfitt et al. 1995; Sumner et al. 2005; Valentine and Gregg 2008; Carracedo-Sánchez et al. 2012; Aravena et al. 2017). Several sedimentary features (e.g., moderate sorting, lack of ash-sized pyroclasts, diffuse stratification, predominance of scoriaceous coarse lapilli & bombs, spindle-shaped agglulinated pyroclasts with ropy outlines) typify distinctive spatter deposits derived from Hawaiian-style lava fountaining elsewhere (Sumner 1998). Furthermore, the coarse-grained size and high vesicularity of the pyroclasts of this phase propose that their deposits have a high volatiles and gas contents as evidenced by the scoriaceous spatter-scoria products, as sign of magmatic fragmentation during Hawaiin activity (e.g., Houghton and Wilson 1989b; Cashman et al. 2014; Mangan and Cashman 1996; Lautze and Houghton 2005; Stovall et al. 2011, 2012).

In addition, the spatter fall deposits of Phase 4 are characterized by the presence of globular cauliflower, bread crust shapes, agglutinated scoria fragments with chilled margin, mantle derived nodules, and a minor proportion of lithic fragments, an suggestive of a rapid cooling and/or magma quenching (White and Valentine 2016; Németh and Kósik, 2020). Abrasion and rounding processes affected most of the juvenile clasts during magmatic fragmentation, as indicated by their spheroidal shapes. This can be elucidated by the fast magma ascent from the source and variations in the eruption style, linked with magma–water interface close to the surface (Houghton and Wilson 1989b; Cashman et al. 2014).

The style of energetic fragmentation together with accretion of gas bubbles and rhythmic expulsions erupted scoriaceous lapilli-bombs, which fell near the vent, constructing spatter deposits during lava fountains (Parfitt and Wilson 1999; Mastin and Ghiorso 2000; Valentine and Gregg 2008). Such style of eruption occurs in hot fluidal state during transport as evidenced by fluidal clasts morphologies (Figs. 9B, 10B) , which allows them to hold heat effectively enough on landing to produce agglutination and rheomorphic/ropy structures that are observed in the studied spatter deposits (Figs. 9G, H, 10A, B).This is facilitated by high rate of mass eruption, accumulation, and temperature of emplacement around the vent, leading to agglutination of magma clots, which perform as viscous flows (Wolff and Sumner 2000; Capaccioni and Cuccoli 2005; Sumner et al. 2005; Carracedo-Sánchez et al. 2012; Kereszturi and Németh 2012a). All these features signify a fluctuation in eruption style, cooling rate, and accretion rate from low to high temperature depositional processes, linked with the outbreak distance of the deposits from the vent (high thermal oxidation; Cashman et al. 2014; Sumner et al. 2005; Valentine and Gregg 2008; Carracedo-Sánchez et al. 2012). In conclusion, Marssous scoria cone seems to have been created by multi-eruptive phases involving phreatomagmatic through Strombolian to Hawaiian activity (e.g., Valentine and Gregg 2008; Guilbaud et al. 2009).

Phase 5: Pahoehoe lava flow (Bpv)

The facies Bpv records the second effusive eruption identified in the Hawaiian succession, characterized by lower effusion and low-explosivity. A diminution in gas content assists a conversion from Hawaiian to lava effusion (Parfitt and Wilson 1995; Valentine and Keating 2007). The presence of a massive, vesicles-rich lava with ropy structure and columnar jointing typifies a pahoehoe lava flow (Rowland and Walker 1987; Self et al. 1996; Schaefer and Kattenhorn 2004). Columnar-jointed lava with rosette (fanning upward) and colonnade joints suggest the lava was formed by several lobes at different stages of cooling which facilitated the vertical lava erosion by prevalent penetration of meteoric water along the columnar joints, creating a laterally quickly changing thermal conditions (cf. Lyle 2000; Harris and Rowland 2009; Sheth et al. 2015; Moore 2019). The record of the vesicles at the base and top of Bpv lava reflects rapid cooling and viscosity increase during lava solidification (Cashman and Kauahikaua 1997).

The appearance of scoriaceous ghosts and vesicular coherent zones close to the spatter-lava transitional contact (Fig.6A), where cooling was faster (e.g., Carracedo-Sánchez et al. 2012; Carracedo Sánchez et al. 2014) refer to a pyroclastic source having fragmentary nature (Fig. 6B) (cf. Sumner 1998; Carracedo-Sánchez et al. 2012). The fabric of scoriaceous clasts/or ghosts (Fig. 6B) in such transition zone (Fig. 6A) is similar to those in the underlying spatter deposits (Unit 3) denote continuous fall deposition of spatter fountains and lava flows, near vent site during a single event in which its clast accumulation rate and temperature oscillated over time, signifying a numerous oscillation in time of the fire fountain (Head and Wilson 1989; Sumner et al. 2005; Carracedo-Sánchez et al. 2012), e.g., the Izu-Oshima volcano, Japan (Sumner, 1998), Summer Coon volcano, Colorado, USA (Valentine et al. 2002). The high rate of both accumulation and spatter coalescence could have sustained spatter-lava interactions and formed a lava lake, behaving as rheomorphic spatter-lava flowage (fire fountains) within maar crater (Sumner et al. 2005; Carracedo-Sánchez et al. 2012), similar to several spatter deposits (e.g., Tenerife, Canary Islands, Gottsmann and Dingwell, 2001; Mayor Island, NewZealand, Gottsmann and Dingwell, 2002; AsamaVolcano, Japan, Yasui and Koyaguchi, 2004). The fluctuation from vuggy spatter to lava-like bodies which includes a discrete welding district between them could be carried out as rafts (Carracedo-Sánchez et al. 2012) inside the flows and conserved within great clasts, denoting the explosive origin and diagnostic identification of fountain-fed flows.

Phase 6: subvolcanic intrusions

The sixth phase represent dike intrusions, an indicative of near-vent and magma cooling during waning phases and terminations of the eruptions. These dikes fed the effusive and pyroclastics that spread along magma-driven fractures (Re et al. 2015), representing the uppermost part of the volcanic edifice. The field observations show the dikes are feeders reached a shallower depth (e.g., vertical dike, Fig. 6D, E) and arrested magma (Geshi et al. 2010) (e.g., ring dike, Fig. 6E). Based on the geometry study of the mafic volcanoes and their plumbing systems, magma may rise via dikes as lava stagnant that emplaced in the growing edifice when magma cools and solidifices inside volcanic cones, extending laterally and vertically many kilometres through the crust from the central conduit (Keating et al. 2008; Pioli

et al. 2008; Carracedo Sánchez et al. 2014; Kereszturi and Németh 2016). Such mechanism is similar to monogenetic mafic fields, in which the lava production pours from the base of the cones (e.g.,Re et al. 2015; Muirhead et al. 2016; Le Corvec et al. 2018).

We visualize that the ring dike (Fig. 6E) is feeder dike because it represents large extended dike (~ 100 m long), parallel to the cone length, and invade the pyroclastic rocks. Several authors noted that feeder dikes progressively bifurcated and broaden upward nearby the surface like ring dike (Fig. 6E) as basaltic eruptions evolve (Keating et al. 2008; Geshi et al. 2010; Harp and Valentine 2015). Well studied mafic dikes feeding scoria cones did not expose into broad bodies until ~ 85 m below surface (Keating et al. 2008), or shallower (~ 15 m; Geshi and Neri 2014). Field remarks on active and extinct volcanoes (e.g., Valentine et al. 2006; Keating et al. 2008; Geshi et al. 2010; Carracedo-Sánchez et al., 2012; Friese et al. 2013) showed that dikes can provide a window into the shallow plumbing systems. Many researchers have linked fluctuating in eruption styles to the geometry of magma plumbing systems (Pioli et al. 2008; Genareau et al. 2010). As respects the pyroclastic dike (Fig. 10G), it is broadly recognised that clastic dikes fill fractures related to very shallow magmatic explosions (e.g., Wolff et al. 1999; Aguirre-Díaz and Labarthe-Hernañdez 2003; Valentine and Krogh 2006; Winter et al. 2008; Lefebvre et al. 2012). The amoeboid edges of the vertical dikes (Fig. 6D) intruded the Unit 3 imply an injection within unconsolidated pyroclastic deposits. Pyroclastic dikes have been observed in modern and ancient explosive volcanic fields (Winter et al. 2008).

Influence of eruptive style and mechanism on pyroclast transport

The exposed pyroclastic deposits consist of complex tephra sequences formed by various mechanisms of fragmentation (Figs. 4, 5). The record of these sequences is due to divergences in eruption's depth and the pre-existing topography (Graettinger et al. 2010). All of these mechanisms organized the ultimate grain size dispersion and textures of the tephra sequences. Furthermore, they influenced the configuration of cone development paths and pyroclast conveyance, such as domination of ballistics, occurrence of convective columns and predominant of grain flows as the result of dissimilar grain-grain collision during transportation and deposition of tephra deposits (Fig. 14, Kereszturi and Németh 2016). The changes in magma flux, which affect the magma fragmentation processes over time, can cause great variation in pyroclastic deposits with substantial variation in grain size and the framework of the pyroclastic succession (Fig. 14, Kereszturi and Németh, 2016).

Marssous deposits were derived from several single or adjoined tephra jets without non-erosive boundaries. Each single jet involved in the expulsion had its own pyroclast-size, profile, and style of expulsion (Graettinger 2018), which marks a unique thickness, runout range, bulk, and architecture on its linked deposit. The grain size and morphology of their pyroclasts change gradually from fine ash (Tb, Unit 1) through lapilli/bombs (LBb, Unit 2) to spatter agglomerates (Bb, Unit 3). Lithofacies Tb, LBb and Bb (see Table 1) signify medial/distal (where fine-grained lithofacies of Tb was generated) to the proximal (as evidenced by massive, coarse and dense pyroclasts of lithofacies LBb and Bb) progression that can be predicated from the exposed tephra jets as revealed by experiments of maar-forming eruption (Graettinger 2018). All happen sequentially from base to top and each has dissimilar proportions of accidental lithic and juvenile clasts, which proposes a composite expulsion and deposition processes via differing depths of eruption. The position of Marssous explosions exposes cyclic alternated pyroclastic deposits from moderately deep sites (where lithofacies Tb are recorded) to less deep sites (lithofacies LBb and Bb) as recorded by the occurrence of accidental-lithic clasts in the former (quartz/feldspar clasts) relative to latter lithofacies Bb (basaltic clasts) via substrate disruption mechanisms.

Phreatomagmatic eruption of Tb lithofacies was emplaced with constrained lateral grain-flows (i.e., laterally moving flows) that was formed by deposition of wet surge deposits (e.g., stratification, cross-bedding, high content of accidental lithics, etc.) belonging to emerging PDCs. The latter can result from hydrovolcanism, even when comparatively small amount of magma is accessible because wet processes are normally more energetic than dry processes. In contrast, the Strombolian/Hawaiian ejection of lithofacies LBb and Bb was generated by the fallout mechanism via the domination of ballistic transportation of coarse clasts in which discrete lava blobs/clasts have no adequate time to cool down and coagulate before landing, establishing rocks with substantial grade of agglutation and coalescence during passing magmatic phases (Fig. 14). The great percentage of coarse clasts can avoid grain avalanching, leading to flank with uneven morphologies (Fig. 14) that are controlled by the accretion rate and temperature of the erupted tephra (e.g., Head and Wilson 1989; Dellino and Volpe 1995, 2000). Furthermore, poor to moderate sorting and whole large size (e.g., coarse lapilli to bombs, Fig. 14) prohibit the grain flow routes on cone flanks that assist to halt gliding and rolling grains (Kereszturi and Németh, 2012a). Such eruptive mechanisms control the scoria cone's geometry (Riedel et al. 2003).

The poor sorting of volcaniclastic sediments create surface roughness (Fig. 14). The medium to coarse lapilli-sized pyroclasts formed by Strombolian-style eruption, can cool down during fallout transportation to generate a granular

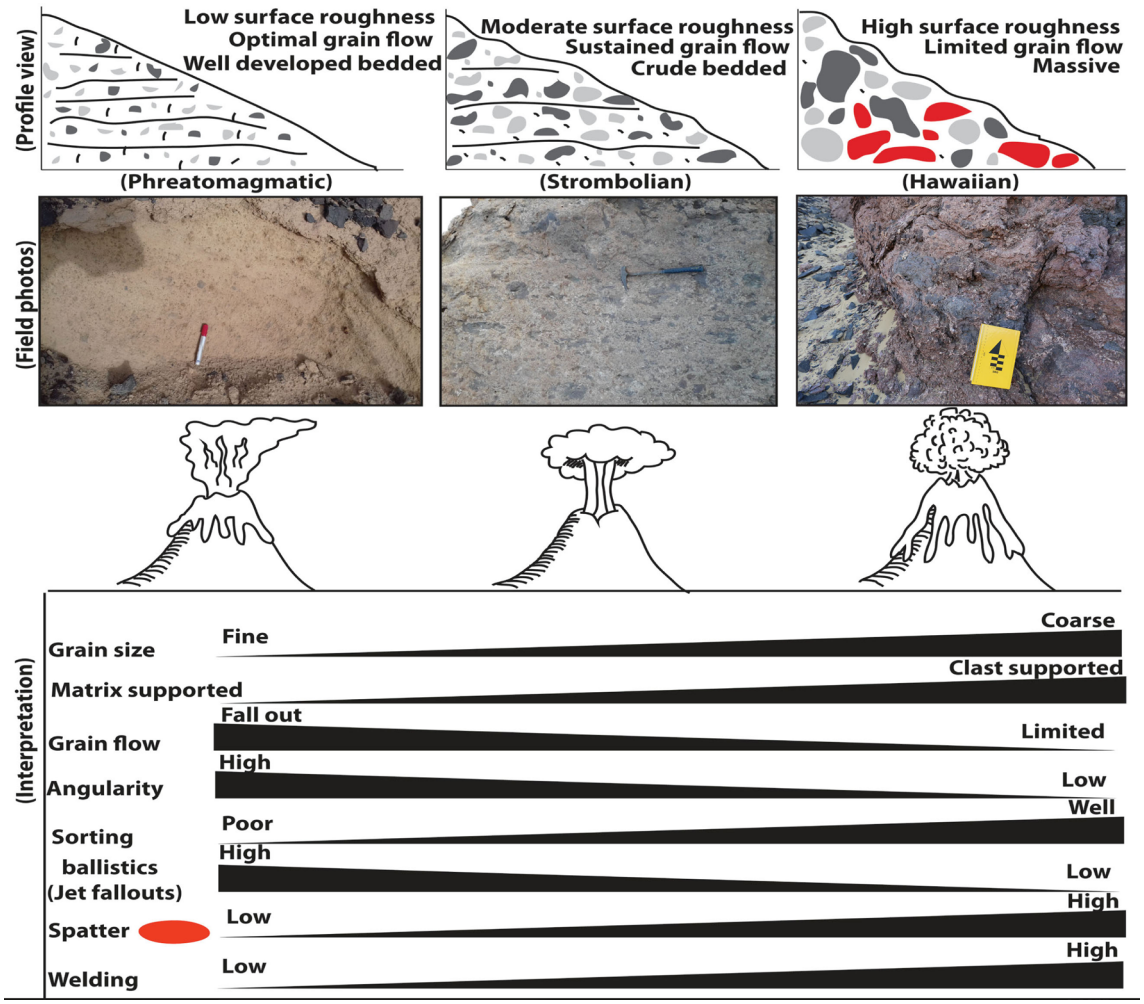

Fig. 14 Effect of eruptive style on transport and mechanism of pyroclastics on the scoria flanks

media on the developing flanks, producing inverse graded deposits (Fig. 8A–C). This confirms that the grains upon landing can preserve their momentum by rolling and gliding on the developing scoria verges (Mitchell 2005; Kereszturi and Németh, 2012b). The obvious unevenness of the depositional surface is low accompanying an increase of grain flow and jet fallouts as the result of the decreasing grain size as phreatomagmatic eruption (e.g., Kereszturi and Németh 2016). Medium to coarse lapilli size with well to moderate sorting can similarly endorse grains to be conveyed downhill by rolling without capture by surface roughness features at the Marssous area (Fig. 14).

In summary, Unit 1 is characterized by strongly altered clay-rich palagonitised deposits compared to the least altered orange and red colored deposits of the both Strombolian (Unit 2) and Hawaiian phase (Unit 3), respectively. The bed thickness and clast size increases from thin Unit 1 (ash to lapilli) through more thick Unit 2 (lapilli-bomb) to Unit 3 (breadcrusted scoriaceous bomb) as an indication of the higher eruptive energy and fragmentation through the initial phreatomagmatic phase having thinly bedded surge deposits and less fragmentation/explosion towards strombolian regime (Unit 2) and the final eruptive phase of Hawaiian activity (Unit 3). Moreover, clasts are extremely angular, less vesicular and more blocky in Unit 1 than the pyroclasts from Unit 2 and Unit 3 of pure magmatic explosions deposits. Clasts become spheroidal-shaped in Unit 3 deposits as derivation from hot-fluid magma. From the combined field, petrographic, and SEM proof, Unit 1 is observed as less vesicularity, blockly angular and extremely fragmented and angular rocks compared with Units 2 and Unit 3, an indicative of water- influenced eruption. The Unit 3 is considered to be a meaningfully less water-affected eruption than Unit 1, evidenced by more spheroidal and ‟fluid-like″ clasts, typical for Hawaiian style. We then deliberate Unit 1 as ″phreatomagmatic", Unit 2 "Strombolian″ and Unit 3 "Hawaiian‟ eruption. These characteristics allowed us to adopt that water-magma mingling diminished and finally

ended completely at the final activity of Gabal Marrsous volcanoes. The entire exposed Marssous deposits are then the mirro of a composite interrelationship of eruptive activities.

Regional implication for monogenetic volcanism

Monogenetic volcanoes may show a widespread variety of eruptive styles, producing diverse volcanic deposites that exhibit a link between the frequency of volcanic eruptions, the eruption volumes, and the complex edifice which would be interpreted as monogenetic or polygenetic volcanoes (Németh 2010; Martí et al. 2016; Valentine et al. 2017). The former erupt within a defined time period without sequential interruption in eruptive history, whereas a latter form in several periods disconnected by distinctive chronological pauses, like paleosols in the stratigraphic succession (Manville et al. 2009; Németh and Kereszturi 2015; Smith and Nemeth 2017). The erraticism and change of various eruptive styles perform a vital function in the building of monogenetic volcanoes (Kereszturi and Németh 2012a, b; Németh and Kereszturi, 2015). The Marssous's scoria cone shows multiple eruptive resemblances with the large complex intracontinental scoria cones in the volcanic fields like Al Haruj volcanic province (AHVP) located in Central Libya, North Africa, predominantly as respects to volcanostratigraphy, eruptive style, and formation of diverse tephra (Németh et al. 2003a; Guilbaud et al. 2009; Alvarado et al. 2011; Agustin-Flores et al. 2011). AHVP is Neogene basaltic scoria cone consisting of a Strombolian and Hawaiin—style eruption, which was followed by hydromagmatic eruption (Németh et al. 2003a; Peregi 2003; Nemeth 2004). Alternative example of various eruptive styles is a scoria cone created by tephra from a weak–phreatomagmatic activity which was followed by a dry magmatic Strombolian activity and lava flows, as recognized from the Al-Duaythah scoria cone, Saudi Arabia (Murcia et al. 2015) and scoria cones from the El Caracol tuff cone and the El Estribo volcano, México (Pola et al. 2015; Kshirsagar et al. 2016). Furthermore, spherical composite lapilli/bombs recorded in Marssous volcano have also been documented in several intraplate alkali mafic scoria cones (Poblete 1995; Ancochea 2004) such as the Calatrava volcanic field, Spain (Cebrià et al. 2000; Carracedo Sánchez et al. 2009, 2017), La Palma, Canary Islands (Schmincke and Sumita 2010), region of Montaña Rajada (Carracedo and Rodríguez 1991), Rothenberg cone in the East Eifel, Germany (Houghton and Schmincke 1989a), and Colli Albani cone, Italy (Sottili et al. 2009).

Based on the volcanic architectures and style of volcanic eruptions, the Marssous complex is a simple monogenetic volcano displaying proof of complex eruptions such as observed at the Al Haruj al Abyad scoria cone, the Al-Duaythah scoria cone, Saudi Arabia or El Caracol tuff cone, Mexico. From these examples, the Marssous complex delivers a chance to investigate the eruptive conditions comprising fragmentation rate, central eruptive mechanisms, and the eruptive outputs produced by dissimilar eruptive styles of isolated magma batches. Furthermore, the Marssous complex provides an idea to comprehend the relation between small–volume magmas, their products and the link with the growth of monogenetic volcanoes. It held continuous effusive and explosive eruptive activity during short time periods without any major episodes of stagnation linked to the magmatic evolution (e.g.,Maro et al. 2017; Ureta et al. 2021). Their eruptive outputs include phreatomagmatic, Strombolian, Hawiian and effusive eruptive styles contributed mainly to tephra ring structure in extensional regime (Houghton et al. 1999; Agustín-Flores et al. 2014). Marssous cone ring is delineated by semi-circular/or ring structures/faults (Figs. 2A–C, 3D), which allow the magma to erupt through these crustal weaknesses (e.g., Valentine and Perry 2007). These ring structures have been recognized in Namibia (e.g., Corner 2000) and Serra Geral Fm, Brazil (Pacheco et al. 2017). Commonly, the ring structures spread over large areas and connected to voluminous intrusive bodies (e.g., Jerram and Bryan 2015), however ring structures linked to a monogenetic volcanic system such as Marssous cone rarely reported. The semi-circular structures are occupied by lava flows and pyroclastic rocks distinguished by facies architecture and sedimentary structures. Pacheco et al. (2017) interpreted the lava lake originated in the semi-circular structure as the central conduits, in which the lake is enriched in fluids and volatiles.The latter were liable for explosive events as verified by the existence of Strombolian and spatter deposits forming vesicles/amygdales-rich scoria cone. In this framework, the Marssous complex could be linked to the NE–SW vent/crater followed from a single monogenetic volcano that was formed in lava lake.

Conclusions

We reported the lithofacies architectures, eruptive mechanisms, and evolution phases of the Gabal Marssous, Bahariya depression, Northwestern Desert of Egypt based on stratigraphic, sedimentological, and volcanological characteristics. The Gabal Marssous is a well-preserved model of Miocene anorogenic alkali mafic scoria cone, resting unconformably on the Bahariya Formation of Upper Cretaceous. The volcanoes of the Marssous scoria cone record periods of continuous multi- evolutionary phases of effusive/explosive volcanic activities without any time gaps, generating different volcanic deposits having variances in their eruptive styles. The latter styles range from effusive through distinct Phreatomagmatic to dry magmatic fall Strombolian and Hawaiian explosive phases that are followed by effusive lavas formed in complex intracone

plumbing system. The fragmentation efficiency decreases, but clast size, grain sorting/roundness, and gain agglutination increase from the onset to the end of the magmatic eruption, constructing spatter-scoria deposits toward the top of the eruptive column. These phases correspond to coherent lava flows and pyroclastic facies associations that are organised in six stages of volcanism and volcaniclastic sedimentation filling the Marssous's crater. They display proof that they were derived from a single eruption emplaced at short times, demonstrating a ″monogenetic volcano‴ style of their edifice growth that displays usual homogeneous in magma composition. The Marssous complex offers a chance for get knowledge about the fluctuations in eruptive styles and their products with referring to the feasible physical procedures (e.g., fragmentation mechanism) that cause the construction of small volume monogenetic volcanoes. The variations in the cone's eruptive styles reflect a wider range of size distributions, grain morphologies, transport mode of ejected pyroclasts, and depositional processes, forming complex volcanic edifice with distinctive pyroclastic deposits at the Marssous complex.

Marssous's magmatic source may have co-existing heterogeneous magmatic pockets, where the cone source originated from changes in feeder system geometry, ascent rates, and dissimilarities in gas-escape efficiency as the result of crystallization (Mastin and Ghiorso 1998; Ross et al. 2008). The deposit's outputs signpost a comparatively fast ascent and an increase in the magma flux/degassing together with variations in the velocity of the upsurge magma and subsequent waning in magma–water interface from wet Phreatomagmatic to magmatic explosive Strombolian and Hawaiin eruptions. All of these influences are supposed to be liable for swift fluctuations in the crystallinity and gas content of the emitted lava, separating ″gas-rich‴ to ″gas-poor‴ products (Cimarelli et al. 2010) and ″wet‴ to ‴dry″ magma flow circumstances (Houghton et al., 1999). In fact, divergences in stratigraphy and hydrogeological characteristics of the substrate, water supply, rock strength and shifts in eruption style show a remarkable function in the architecture of the Marssous scoria cone, as has been documented at corresponding volcanic regions and other monogenetic centers elsewhere (Valentine et al. 2006; Auer et al. 2007; Pioli et al. 2008).

Supplementary Information The online version contains supplementary material available at https://doi.org/10.1007/s00531-021-02099-5.

Acknowledgements This paper is a part of the Master Thesis by Azeeza Maged at Cairo University, Faculty of Science, Giza, Egypt. Financial support by the Cairo University is acknowledged. We acknowledge the help of Dr. Sano during XRF and ICP-MS analyses. Insightful reviews by Vladislav Rapprich and Raymond Duraiswami as well as the constructive suggestions from the editor Wolf-Christian Dullo are gratefully acknowledged.

References

Abdel Aal AY (1998) Mineral and chemical composition of basalts in the neighbourhood of Giza, Egypt. J Afr Earth Sci 26:101–117

Agostini S, Ronca S, Bellon H, Luciani N, Lustrino M (2016) The Oligo-Miocene alkaline volcanism of Bahariya depression, Western Desert, Egypt. Italian Society of Mineralogy and Petrology (SIMP). IGG, CNR-Pisa

Aguirre-Díaz G, Labarthe-Hernañdez G (2003) Fissure ignimbrites: fissure-source origin for voluminous ignimbrites of the Sierra Madre Occidental and its relationship with Basin and Range faulting. Geol 31:773–776

Agustin-Flores J, Siebe C, Guilbaud M-N (2011) Geology and geochemistry of Pelagatos, Cerro del Agua, and Dos Cerros monogenetic volcanoes in the Sierra Chichinautzin volcanic field, south of Mexico City. J Volcanol Geotherm Res 201(1–4):143–162

Agustín-Flores J, Németh K, Cronin SJ, Lindsay JM, Kereszturi G, Brand BD, Smith IE (2014) Phreatomagmatic eruptions through unconsolidated coastal plain sequences, Maungataketake, Auckland volcanic field (New Zealand). J Volcanol Geoth Res 276:46–63

Alvarado G, Pérez W, Vogel T, Gröger H, Patiño L (2011) The Cerro Chopo basaltic cone (Costa Rica): an unusual completely reversed graded pyroclastic cone with abundant low vesicular cannonball juvenile fragments. J Volcanol Geotherm Res 201:163–177

Ancochea E (2004) La región volcánica del Campo de Calatrava. In: Vera JA (ed) Geología de España. SGE-IGME, Madrid, pp 676–677

Andronico D, Cristaldi A, Scollo S (2008) The 4–5 September 2007 lava fountain at south-east crater of Mt Etna. Italy J Volcanol Geotherm Res 173:325–328

Aravena Á, Vitturi MDM, Cioni R, Neri A (2017) Stability of volcanic conduits during explosive eruptions. J Volcanol Geotherm Res 339:52–62

Auer A, Martin U, Németh K (2007) The Fekete-hegy (Balaton Highland Hungary) "softsubstrate" and "hard-substrate" maar volcanoes in an aligned volcanic complex implications for vent geometry, subsurface stratigraphy and the palaeoenvironmental setting. J Volcanol Geotherm Res 159:225–245

Baldridge WS, Eyal Y, Bartov Y, Steinitz G, Eyal M (1991) Miocene magmatism of Sinai related to the opening of the Red Sea. Tectonophysics 197:181–201

Bélanger C, Ross PS (2018) Origin of nonbedded pyroclastic rocks in the Cathedral Cliff diatreme, Navajo volcanic field, New Mexico. Bull Volcanol 80:61

Belousov A, Belousova M (2018) Dynamics and viscosity of 'a'a and pahoehoe lava flows of the 2012–2013 eruption of Tolbachik volcano, Kamchatka (Russia). Bull Volcanol 80(1):6

Bosworth W (1992) Mesozoic and early Tertiary rift tectonics in east Africa. Tectonophy 209:115–137

Bosworth W, William J (2015) Geological evolution of the red sea: historical background, review, and synthesis. In: Rasul N, Stewart CF (eds) The red sea—the formation, morphology, oceanography and environment of a young ocean basin. https://doi.org/10.1007/978-3-662-45201-1

Bosworth W, Stockli DF (2016) Early magmatism in the greater Red Sea rift: timing and significance. Can J Earth Sci 53:1158–1176

Bosworth W, Huchon P, McClay K (2005) The Red Sea and Gulf of Aden basins. J Afri Earth Sci 43(1–3):334–378

Bosworth W, El-Hawat AS, Helgeson DA, Burke K (2008) Cyrenaican "shock absorber" and associated inversion strain shadow in the collision zone of northeast Africa. Geol 36(9):695–698
Bosworth W, Stockli DF, Helgeson DE (2015) Integrated 1 outcrop, 3D seismic, and geochronologic interpretation of Red Sea dike-related deformation in the Western Desert, Egypt —the role of the 23 Ma Cairo "mini-plume". J Afri Earth Sci 109:107–119
Branney MJ, Kokelaar P (1992) A reappraisal of ignimbrite emplacement: progressive aggradation and changes from particulate to nonparticulate flow during emplacement of high-grade ignimbrite. Bull Volcanol 54(6):504–520
Brand BD, Clarke AB, Semken S (2014) Eruptive conditions and depositional processes of Narbona Pass Maarvolcano, Navajo volcanic field, Navajo Nation, New Mexico (USA). Bull Volcanol 71:49–77
Brenna M, Croning SJ, Smith EM, Sohn SY, Nemeth K (2010) Mechanisms driving polymagmatic activity at a monogenetic volcano, Udo, Jeju Island, South Korea. Contrib Mineral Petrol 160:931–950
Brenna M, Croning SJ, Smith EM, Sohn SY (2011) The influence of magma plumbing complexity on monogenetic eruptions, Udo, Jeju Island. South Korea Terra Nova 23:70–75
Bryan SE, Ernst RE (2008) Revised definition of large Igneous Provinces (LIPs). Earth Sci Rev 86:175–202
Buettner R, Dellino P, La Volpe L, Lorenz V, Zimanowski B (2002) Thermohydraulic explosions in phreatomagmatic eruptions as evidenced by the comparison between pyroclasts and products from Molten Fuel Coolant Interaction experiments. J Geophys Res 107:1–14. https://doi.org/10.1029/2001JB000511
Burke K (1996) The African plate. South African J Geol 99(4):341–409
Camp VE, Roobol MJ (1992) Upwelling asthenosphere beneath western Arabia and its regional implication. J Geophys Res 97:15255–15271
Cañón-Tapia E (2016) Reappraisal of the significance of volcanic fields. J Volcanol Geotherm Res 310:26–38
Capaccioni B, Cuccoli F (2005) Spatter and welded air fall deposits generated by firefountaining eruptions: cooling of pyroclasts during transport and deposition. J Volcanol Geotherm Res 145(3):263–280
Carracedo JC, Rodríguez E (1991) Lanzarote. La erupción volcánica de 1730. Servicio de Publicaciones, Cabildo Insular de Lanzarote
Carracedo Sánchez M, Sarrionandia F, Arostegui J, Larrondo E, Gil Ibarguchi JI (2009) Development of spheroidal composite bombs by welding of juvenile spinning and isotropic droplets inside a mafic eruption column. J Volcanol Geotherm Res 186:265–279
Carracedo Sánchez M, Arostegui J, Sarrionandia F, Larrondo E, Gil Ibarguchi JI (2010) Cryptoachneliths: hidden glassy ash in composite spheroidal lapilli. J Volcanol Geotherm Res 196:77–90
Carracedo Sánchez M, Sarrionandia F, Gil Ibarguchi JI (2014) Post-depositional intrusion and extrusion through a scoria and spatter cone of fountain-fed nephelinite lavas (Las Herrerías volcano, Calatrava, Spain). Bull Volcanol 76:860. https://doi.org/10.1007/s00445-014-0860-4
Carracedo-Sánchez M, Sarrionandia F, Arostegui J, Eguiluz L, Gil Ibarguchi JI (2012) The transition of spatter to lava-like body in lava fountain deposits: features and examples from the Cabezo Segura volcano (Calatrava, Spain). J Volcanol Geotherm Res 227–228:1–14
Carracedo-Sánchez M, Sarrionandia F, Arostegui J, Gil Ibarguchi JI (2015) Silicate glass micro and nanospherules generated in explosive eruptions of ultrabasicmagmas: implications for the origin of pelletal lapilli. J Volcanol Geotherm Res 293:13–24
Carracedo-Sancheza M, Sarrionandiab F, Abalosc B, Errandonea-Martina J, Gil Ibarguchia JI (2017) Intra-cone plumbing system and eruptive dynamics of smallvolume basaltic volcanoes: a case study in the Calatrava Volcanic Field. J Volcanol Geoth Res 348:82–95
Cas RAF, Wright JV (1987) Volcanic successions. Allen & Unwin, London
Cashman KV, Kauahikaua JP (1997) Reevaluation of vesicle distributions in basaltic lava flows. Geology 25(5):419–422
Cashman KV, Mangan MT, Poland MP, Takahashi TJ, Landowski CM (2014) A century of studying effusive eruptions in Hawai. Characteristics of Hawaiian Volcanoes. p 357
Cebrià JM, Lopèz-Riuz J, Doblas M, Oyarzun R, Hetogen J, Benito R (2000) Geochemestry of the Quaternary alkali basalts of Garrotxa (NE Volcanic Province, Spain): a case of double enrichment of the mantle lithosphere. J Volcanol Geotherm Res 102:217–235
Chough SK, Sohn YK (1990) Depositional mechanics and sequences of base surges, Songaksan tuff ring, Cheijn Island, Korea. Sedimentology 37:1115–1135
Cimarelli C, Di Traglia F, Taddeucci J (2010) Basaltic scoria textures from a zoned conduit as precursors to violent strombolian activity. Geology 38(5):439–442
Cioni R, Marianelli P, Sbrana A (1992) Dynamics of the AD 79 eruption: stratigraphic, sedimentological and geochemical data on the successions from the Somma-Vesuvius southern and eastern sectors. Acta Vulcanol 2:109–123
Clarke H, Troll VR, Carracedo JC (2009) Phreatomagmatic to Strombolian eruptive activity of basaltic cindercones:-Montana Los Erales, Tenerife Canary Island. J Volcanol Geotherm Res 180:225–245
Collinson JD (1969) The sedimentology of the GrindslowShales and the Kinderscout Grit: a deltaic complex in the Namurian of northern England. J Sediment Res 39(1):1–23
Collinson JD (1996) Alluvial sediments. In: Reading HG (ed) Sedimentary environments and facies, 3rd edn. Blackwell Publishing, Oxford, pp 37–82
Corner B (2000) Crustal framework of Namibia derived from magnetic and gravity data. Commun Geol Survey Namibia 12:13–19
Dalrymple RW (2010) Interpreting sedimentary successions: facies, facies analysisi and facies models. Facies Models 4(2):3–18
Dellino P, La Volpe L (1995) Fragmentation versus transportation mechanisms in the pyroclastic sequence of Monte Pilato — Rocche Rosse (Lipari, Italy). J Volcanol Geotherm Res 64:211–232
Dellino P, La Volpe L (2000) Structures and grain size distribution in surge deposits as a tool for modelling the dynamics of dilute pyroclastic density currents at La Fossa di Vulcano (Aeolian Islands, Italy). J Volcanol Geotherm Res 96:57–78
El Aref MM, Abou Khadrah MA, Lotfi ZH (1987) Karst topography and karstification processes in the Eocene limestone plateau of El Bahariya Oasis, Western Desert. Egypt J Geomorph 31:45–64
El Aref MM, El Dougdog AA, Mesaed AA (1991) Landform evolution and formation of ferricrete duricrusts, El Heiz Area, El Bahariya depression, Western Desert. Egypt J Geol 34:1–39
El Aref MM, Hammed MS, Salama A (2017) Inventory and assessment of the geomorphosites of Bahariya-Farafra Territory, Western Desert. Egypt Int J Sci Basic Appl Res 33:128–143
El Ghamry MN, El Amawy M, Hagag W (2020) The role of Late Cretaceous wrench tectonics in hydrocarbon endowment in El-Gindi Basin, northern Western Desert, Egypt. Mar Pet Geol 112:104093
Endress C, Furman T, Abu El-Rus MA (2009) Geochemistry of 24 Ma Basalts from Northeast Egypt: Implications for Small-Scale Convection Beneath the East African Rift System. Amer. Geophys. Union (AGU)
Endress C, Furman T, Abu El-Rus MA, Hanan BB (2011) Geochemistry of 24 Ma basalts from NE Egypt: source components and fractionation history. In: Van Hinsbergen DJJ, Buiter SJH, Torsvik TH, Gaina C, Webb SJ (eds) The Formation and

Evolution of Africa: a Synopsis of 3.8 Ga of Earth History. Geol Soci Lond Sp Publ 357:265–283
Fisher RV, Waters AC (1970) Base surge bed forms in maar volcanoes. Am J Sci 268:157–180
Fisher RV, Schmincke HU (1984) Pyroclastic rocks. Springer-Verlag, New York
Friese N, Bense FA, Tanner DC, Gústafsson LE, Siegesmund S (2013) From feeder dykes to scoria cones: the tectonically controlled plumbing system of the Rauðhólar volcanic chain, Northern Volcanic Zone. Icel Bull Volc 75:1–19
Geshi N, Neri N (2014) Dynamic feeder dike systems in basaltic volcanoes: the exceptional example of the 1809 Etna eruption (Italy). Front Earth Sci 2(13):1–11. https://doi.org/10.3389/feart.2014.00013
Geshi N, Kusumoto S, Gudmundsson A (2010) Geometric difference between nonfeeder and feeder dikes. Geology 38(3):195–198
González G, Cembrano J, Aron F, Veloso EE, Shyu JBH (2019) Coeval compressional deformation and volcanismin the central Andes, case studies from northern Chile (23S–24S). Tectonics 28, TC6003
Gottsmann J, Dingwell DB (2001) Cooling dynamics of spatter-fed phonolite obsidian flows on Tenerife, Canary Islands. J Volcanol Geotherm Res 105(4):323–342
Gottsmann J, Dingwell DB (2002) The thermal history of a spatter-fed lava flow: the 8-ka pantellerite flow of Mayor Island, New Zealand. Bull Volcanol 64(6):410–422
Graettinger AH (2018) Trends in maar crater size and shape using the global Maar Volcano Location and Shape (MaarVLS) database. J Volcanol Geotherm Res 357:1–13. https://doi.org/10.1016/j.jvolgeores.2018.04.002
Graettinger AH, Valentine GA (2017) Evidence for the relative depths and energies of phreatomagmatic explosions recorded in tephra rings. Bull Volcanol 79(12):88. https://doi.org/10.1007/s00445-017-1177-x
Graettinger AH, Manville V, Briggs RM (2010) Depositional record of historic lahars in the upper Whangaehu Valley, Mt. Ruapehu, New Zealand: implications for trigger mechanisms, flow dynamics and lahar hazards. Bull Volcanol 72(3):279–296
Guilbaud MN, Siebe C, Agustín-Flores J (2009) Eruptive style of the young high-Mg basaltic–andesite Pelagatos scoria cone, southeast of México City. Bull Volcanol 71:859–880
Guiraud R, Bosworth W (1997) Senonian basin inversion and rejuvenation of rifting in Africa and Arabia:-synthesis and implications to plate-scale tectonics. Tectonophysics 282:39–82
Guiraud R, Bosworth W, Thierry J, Delphanque A (2005) Phanerozoic geological evolution of northern and central Africa: overview. J Afr Earth Sci 43:83–143
Gurioli L, Colò L, Bollasina AJ, Harris AJL, Whittington A, Ripepe M (2014) Dynamics of Strombolian explosions: inferences from field and laboratory studies of erupted bombs from Stromboli volcano. J Geophys Res Solid Earth 119(1):319–345
Harp AG, Valentine GA (2015) Shallow plumbing and eruptive processes of a scoria cone built on steep terrain. J Volcanol Geotherm Res 294:37–55
Harris AJL, Rowland SK (2009) Effusion rate controls on lava flow length and the role of heat loss: a review. In: Hoskuldsson A, Thordarson T, Larsen G, Self S, Rowland S (eds) The legacy of George P.L Walker, Special Publications of IAVCEI 2. Geol. Soci. of London, London, pp 33–51
Head JW, Wilson L (1989) Basaltic pyroclastic eruptions: influence of gas-release patterns and volume fluxes on fountain structure, and the formation of cinder cones, spatter cones, rootless flows, lava ponds and lava flows. J Volcanol Geotherm Res 37(3–4):261–271
Heiken G (1972) Morphology and petrography of volcanic ashes. Geol Soc Am Bull 83:1961–1988
Heiken G (1974) An atlas of volcanic ash. Smithson Contrib Earth Sci 12:1–101
Heiken G, Wohletz K (1991) Volcanic ash. University of California Press, Berkeley
Hon K, Kauahikaua J, Denlinger R, McKay K (1994) Emplacement and inflation of pahoehoe sheet flows observation and measurements of active lavas on Kilauea volcano, Hawaii. Geol Soc Am Bull 106:351–370
Honnorez J, Kirst P (1975) Submarine basaltic volcanism: morphometric parameters for discriminating hyaloclastites from hyalotuffs. Bull Volcanol 32:441–465
Houghton BF, Gonnermann HM (2008) Basaltic explosive volcanism: constraints from deposits and models. Chem Erde Geochem 68:117–140
Houghton BF, Hackett WR (1984) Strombolian and phreatomagmatic deposits of Ohakune craters, Ruapehu, New Zealand: a complex interaction between external water and rising basaltic magma. J Volcanol Geotherm Res 21(3–4):207–231
Houghton BF, Schmincke HU (1989a) Rothenberg scoria cone, East Eifel: a complex Strombolian and phreatomagmatic volcano. Bull Volcanol 52:28–48
Houghton BF, Wilson CJN (1989b) A vesicularity index for pyroclastic deposits. Bull Volcanol 51(6):451–462
Houghton BF, Smith RT (1993) Recycling of magmatic clasts during explosive eruptions—estimating the true juvenile content of phreatomagmatic volcanic deposits. Bull Volcanol 55(6):414–420
Houghton BF, Wilson CJN, Rosenberg MD, Smith IEM, Parker RJ (1996) Mixed deposits of complex magmatic and phreatomagmatic volcanism: an example from Crater Hill, Auckland, New Zealand. Bull Volcanol 58:59–66
Houghton BF, Wilson CJN, Smith IEM (1999) Shallow-seated controls on styles of explosive basaltic volcanism: a case study from New Zealand. J Volcanol Geotherm Res 91(1):97–120
Houghton BF, Wilson CJN, Del Carlo P, Coltelli M, Sable JE, Carey R (2004) The influence of conduit processes on changes in style of basaltic Plinian eruptions Tarawera 1886 and Etna 122 BC. J Volcanol Geotherm Res 137:1–17
Ilani S, Harlavan Y, Tarawneh K, Rabba I, Weinberger R, Ibrahim K, Peltz S, Steinitz G (2001) New K-Ar ages of basalts from the Harrat Ash Shaam volcanic field in Jordan: implications for the span and duration of the upper-mantle upwelling beneath the western Arabian plate. Geology 29:171–174
Jerram DA, Bryan SE (2015) Plumbing systems of shallow level intrusive complexes. Springer, Advances in Volcanology, pp 1–22
Johnson SY (1989) Significance of loessite in the Maroon Formation (Middle Pennsylvanian to Lower Permian), Eagle Basin, northwest Colorado. J Sed Petrol 59:782–791
Johnson JS, Smellie JL (2007) Zeolite compositions as proxies for eruptive paleoenvironment. Geochem Geophys Geosyst. https://doi.org/10.1029/2006GC001450)
Johnson P, Valentine G, Cortés J, Tadini A (2014) Basaltic tephra from monogenetic Marcath Volcano, central Nevada. J Volcanol Geotherm Res 281:27–33
Junqueira-Brod TC, Brod JA, Thompson RN, Gibson SA (1999) Spinning droplets—a conspicuous lapilli-size structure in kamafugite diatremes of southern Goiás. Brazil Rev Brasileira de Geociencias 29(3):437–440
Keating GN, Valentine GA, Krier DJ, Perry FV (2008) Shallow plumbing systems for small-volume basaltic volcanoes. Bull Volcanol 70:563–582
Kereszturi G, Németh K (2012a) Monogenetic basaltic volcanoes: genetic classification, growth, geomorphology and degradation. In: Németh K (ed) Updates in volcanology— new advances in understanding volcanic systems. InTech, pp 3–88. https://doi.org/10.5772/51387 (**ISBN: 978-953-51-0915-0**)

Kereszturi G, Németh K (2012b) Structural and morphometric irregularities of eroded Pliocene scoria cones at the Bakony-Balaton highland volcanic field, Hungary. Geomorphology 136(1):45–58

Kereszturi G, Németh K (2016) Sedimentology, eruptive mechanism and facies architecture of basaltic scoria cones from the Auckland Volcanic Field (New Zealand). J Volcanol Geotherm Res 324:41–56

Kereszturi G, Csillag G, Nemeth K, Sebe K, Balogh K, Jager V, Pecskay Z (2012) Volcanic architecture, eruption mechanism and landform evolution of a Plio/Pleistocene intracontinental basaltic polycyclic monogenetic volcano from the Bakony-Balaton Highland volcanic field, Hungary. Cent Eur J Geosci 2(3):362–384

Khalaf EA, Hammed MS (2016) Morphology and development of pahoehoe flow-lobe tumuli and associated features from a monogenetic basaltic volcanic field, Bahariya Depression, Western Desert, Egypt. J Afr Earth Sci 113:165–180

Khalaf EA, Sano T (2020) Petrogenesis of Neogene polymagmatic suites at a monogenetic low-volume volcanic province, Bahariya depression, Western Desert, Egypt. Intern J Earth Sci 109:995–1027. https://doi.org/10.1007/s00531-020-01849-1

Khalaf EA, Abdel Wahed M, Mayed A, Mokhtar H (2019) Volcanic Geosites and Their Geoheritage Values Preserved in Monogenetic Neogene Volcanic Field, Bahariya Depression, Western Desert, Egypt: Implication for Climatic Change-Controlling Volcanic Eruption. Geoheritage 11:855–873. https://doi.org/10.1007/s12371-018-0336-6

Kienle J, Kyle PR, Self S, Motyka RJ, Lorenz V (1980) Ukinrek Maars, Alaska, I. April 1977 eruption sequence, petrology and tectonic setting. J Volcanol Geotherm Res 7:11–37

Kosik S, Nemeth K, Kereszturi G, Procter JN, Zellmer GF, Geshi N (2016) Phreatomagmatic and water-influenced Strombolian eruptions of a small-volume parasitic cone complex on the southern ringplain of Mt. Ruapehu, New Zealand: Facies architecture and eruption mechanisms of the Ohakune Volcanic Complex controlled by an unstable fissure eruption. J Volcanol Geotherm Res 327:99–115

Kshirsagar P, Siebe C, Guilbaud MN, Salinas S (2016) Geological and environmental controls on the change of eruptive style (phreatomagmatic to Strombolian effusive) of late Pleistocene El Caracol tuff cone and its comparisonwith adjacent volcanoes around the Zacapu basin (Michoacán, México). J Volcanol Geoth Res 318:114–133

Latutrie B, Ross PS (2018) Lava lakes filling phreatomagmatic craters at Twin Peaks, Hopi Buttes volcanic field, Navajo Nation, Arizona. Seventh International Maar Conference, Olot

Latutrie B, Ross PS (2019) Transition zone between the upper diatreme and lower diatreme: origin and significance at Round Butte, Hopi Buttes volcanic field, Navajo Nation, Arizona. Bull Volcanol 81:26

Lautze NC, Houghton BF (2005) Linking variable explosion style and magma textures during 2002 at Stromboli volcano. Italy Bull Volcanol 69:445–460

Le Corvec N, Muirhead JD, White JDL (2018) Shallow magma diversions during explosive diatreme-forming eruptions. Nat Commun 9:1459

Lefebvre NS, White JDL, Kjarsgaard BA (2012) Unbedded diatreme deposits reveal maar-diatreme-forming eruptive processes: Standing Rocks West, Hopi Buttes, Navajo Nation, USA. Bull Volcanol 75:1–17

Lefebvre NS, White JDL, Kjarsgaard BA (2016) Arrested diatreme development: Standing Rocks East, Hopi Buttes, Navajo Nation, USA. J Volcanol Geotherm Res 310:186–208

Lefebvre NS (2013) Volcanology of maar-diatreme volcanic vent complexes, Hopi Buttes Volcanic Field, Navajo Nation,Arizona, USA. Unpubl PhD thesis, Otago Univ, New Zealand

Ligi M, Bonatti E, Bosworth W, Cai Y, Cipriani A, Palmiotto C, Ronca S, Seyler M (2018) Birth of an ocean in the Red Sea: oceanic-type basaltic melt intrusions precede continental rupture. Gond Res 54:150–160

Long PE, Wood BJ (1986) Structures, textures, and cooling histories of Columbia River basalt flows. Geol Soc Am Bull 97:1144–1155

Lorenz V (1985) Maars and diatremes of phreatomagmatic origin: a review. Trans Geol Soc S Afr 88:459–470

Lorenz V (1986) On the growth of maars and diatremes and its relevance to the formation of tuff rings. Bull Volcanol 48:265–274

Lorenz V (1987) Phreatomagmatism and its relevance. Chem Geol 62(1–2):149–156

Lorenz V (2000) Formation of maar–diatreme volcanoes. Terra Nostra 2000(6):284–291

Lustrino M, Wilson M (2007) The circum-Mediterranean anorogenic Cenozoic igneous province. Earth Sci Rev 81:1–65

Lyle P (2000) The eruption environment of multi-tiered columnar basalt lava flows. J Geol Soc Lond 157:715–722

Ma L, Jiang SY, Hofmann AW, Xu YG, Dai BZ, Hou ML (2016) Rapid lithospheric thinning of the North China craton: new evidence from cretaceous mafic dikes in the Jiaodong Peninsula. Chem Geol 432:1–15

Mangan MT, Cashman KV (1996) The structure of basaltic scoria and reticulite and inferences for vesiculation, foam formation, and fragmentation in lava fountains. J Volcanol Geotherm Res 73:1–18

Manville V, Németh K, Kano K (2009) Source to sink: a review of three decades of progress in the understanding of volcaniclastic processes, deposits, and hazards. Sediment Geol 220:136–161

Maro G, Caffe PJ (2016) Neogene monogenetic volcanism from the Northern Puna region: products and eruptive styles. In: Németh K, Carrasco-Núñez G, Aranda- Gómez JJ, Smith IEM (eds) Monogenetic volcanism. Geol Scoi, London, pp 337–359. https://doi.org/10.1144/sp446.6

Maro G, Caffe PJ, Romer R, Trumbull RB (2017) Neogene mafic magmatism in the Northern Puna Plateau, Argentina: generation and evolution of a back-arc volcanic suite. J Pet 58(8):1591–1617. https://doi.org/10.1093/petrology/egx066

Martin U, Németh K (2005) Eruptive and depositional history of a Pliocene tuff ring that developed in a fluvio-lacustrine basin: Kissomlyó volcano (western Hungary). J Volcanol Geotherm Res 147(3):342–356

Martin U, Nemeth K (2006) How Strombolian is a Strombolian- scoria cone? Some irregularities in scoria cone architecture from the Transmexican Volcanic Belt, near Volcán Ceboruco, (Mexico) and Al Haruj (Libya). J Volcanol Geotherm Res 155:104–118

Mastin LG, Ghiorso MS (1998) Adiabatic temperature changes of magma-gas mixtures during volcanic eruptions. Eos Trans AGU 79(45)

Mastin L, Ghiorso M (2000) A numerical program for steady-state flow of magma–gas mixtures through vertical eruptive conduits. U. S. Geological Survey Open-file Report No. 209

Martí J, Planagumà L, Geyer A, Canal E, Pedrazzi D (2016) Complex interaction between Strombolianandphreatomagmatic eruptions in the Quaternary monogenetic volcanism of the Catalan Volcanic Zone (NE of Spain). J Volcanol Geotherm Res 201:178–193

Mazzarini F, Rooney TO, Isola I (2013) The intimate relationship between strain and magmatism: a numerical treatment of clustered monogenetic fields in the Main Ethiopian Rift. Tectonics 32:49–64

Mazzini A, Lupi M, Sciarra A, Hammed M, Schmidt ST, Suessenberger A (2019) Concentric structures and hydrothermal venting in the Western Desert. Egypt Front Earth Sci. https://doi.org/10.3389/feart.2019.00266

Mcdonald GA (1972) Volcanoes. Prentice-Hall Inc., Englewood Cliffs

McGee L, Smith IEM (2016) Interpreting chemical compositions of small scale basaltic systems: a review. J Volcanol Geotherm Res 325:45–60. https://doi.org/10.1016/j.jvolgeores.2016.06.007
McGetchin TR, Settle M, Chouet BA (1974) Cinder cone growth modeled after northeast crater, Mount Etna, Sicily. J Geophys Res 79(23):3257–3272
McPhie J, Doyle M, Allen R (1993) Volcanic textures: a guide to the interpretation of textures in volcanic rocks. CODES, Univ Tasmania, Berlin, p 196
Meneisy MY (1990) Vulcanicity. In: Said R (ed) The geology of Egypt. Balkema, Rotterdam, pp 157–172
Meschede M (1986) A method of discriminating between different types of mid-Ocean ridge basalts and continental tholeiites with the Nb-Zr-Y diagram. Chem Geol 56:207–218
Mitchell KL (2005) Coupled conduit flow and shape in explosive volcanic eruptions. J Volcanol Geotherm Res 143(1–3):187–203
Moore JG (2019) Mini-columns and ghost columns in Columbia River lava. J Volcanol Geotherm Res 374:242–251
Moustafa AR, Saoudi A, Moubasher A, Ibrahim IM, Molokhia H, Schwartz B (2003) Structural setting and tectonic evolution of the Bahariya Depression, Western Desert. Egypt. Geoarabia 8(1):91–124 (**Gulf Petrolink, Bahrain**)
Muirhead JD, Van Eaton AR, Re G, White JDL, Ort MH (2016) Monogenetic volcanoes fed by interconnected dikes and sills in the Hopi Buttes volcanic field, Navajo Nation, USA. Bull Volcanol 78:1–16
Murcia H, Németh K (2020) Effusive monogenetic volcanism. In: Németh K (ed) Volcanoes-updates in volcanology. IntechOpen, Rijeka. https://doi.org/10.5772/intechopen.94387
Murcia H, Németh K, El-Masry NN, Lindsay JM, Moufti MRH, Wameyo P, Cronin SJ, Smith IEM, Kereszturi G (2015) The Al-Du'aythah volcanic cones, Al-Madinah City: implications for volcanic hazards in northern Harrat Rahat, Kingdom of Saudi Arabia. Bull Volcanol 77(6):1–19
Murtagh RM, White JDL (2013) Pyroclast characteristics of a subaqueous to emergent Surtseyan eruption, Black Point volcano, California. J Volcanol Geotherm Res 267:75–91. https://doi.org/10.1016/j.jvolgeores.2013.08.015
Németh K (2010) Monogenetic volcanic fields: origin, sedimentary record, and relationship with polygenetic volcanism. Geol Soc Am Sp Pap 470:43–66
Németh K, Kereszturi G (2015) Monogenetic volcanism: personal views and discussion. Int J Earth Sci 104:2131–2146
Németh K, Kósik S (2020) Review of explosive hydrovolcanism. Geosciences 10(2):44
Németh K, Martin U (2007) Shallow sill and dyke complex in western Hungary as a possible feeding system of phreatomagmatic volcanoes in "soft-rock" environment. J Volcanol Geotherm Res 159:138–152. https://doi.org/10.1016/j.jvolgeores.2006.06.014
Németh K, Martin U, Harangi S (2001) Miocene phreatomagmatic volcanism at Tihany (Pannonian Basin, Hungary). J Volcanol Geotherm Res 111(1–4):111–135
Németh K, Suwesi KS, Peregi Z, Gulácsi Z, Ujszászi J (2003a) Plio/pleistocene flood basalt related scoria and spatter cones, rootless lava flows, and pit craters, Al Haruj Al Abiyad, Libya. Geolines J Geol Inst AS Czech Repub 15:98–103
Németh K, White JDL, Reay A, Martin U (2003b) Compositional variation during monogenetic volcano growth and its implications for magma supply to continental volcanic fields. J Geol Soci Lond 160(4):523–530
Németh K, Risso C, Nullo F, Kereszturi G (2011) The role of collapsing and cone rafting on eruption style changes and final conemorphology: LosMorados scoria cone, Mendoza, Argentina. Cent Eur J Geosci 3(2):102–118
Nemeth K (2004) The morphology and origin of wide craters at Al Haruj al Abyad, Libya: maars and phreatomagmatism in a large intracontinental flood lava field? Z Fur Geomorphol 48(4):417–439
Nemeth K, Kosik S (2020) The role of hydrovolcanism in the formation of the Cenozoic monogenetic volcanic fields of Zealandia. N Z J Geol Geophys 63(4):402–427
Pacheco FERC, Caxito FA, Moraes LC, Marangoni YR, Santos RPZ, Soares ACP (2017) Basaltic ring structures of the Serra Geral Formation at the southern Triângulo Mineiro, Água Vermelha region, Brazil. J Volcanol Geotherm Res. https://doi.org/10.1016/j.jvolgeores.2017.06.019
Parfitt EA (2004) A discussion of the mechanisms of explosive basaltic eruptions. J Volcanol Geotherm Res 134(1–2):77–107
Parfitt EA, Wilson L (1995) Explosive volcanic eruptions—IX. The transition between Hawaiian-style lava fountaining and Strombolian explosive activity. Geophys J Int 121:226–232
Parfitt EA, Wilson L (1999) A Plinian treatment of fallout from Hawaiian lava fountains. J Volcanol Geotherm Res 88:67–75
Parfitt EA, Wilson L, Neal CA (1995) Factors influencing the height of Hawaiian lava fountain: implication for the use of fountain height as an indicator of magma gas content. Bull Volcanol 57:440–450
Pearce JA (1996) A user's guide to basalt discrimination diagrams. In: Wyman DA (ed) Trace element geochemistry of volcanic rocks. Application for massive sulphide exploration. Geol Assoc Canada 12:79–113
Pedrazzi D, Bolós X, Barde-Cabusson S, Martí J (2016) Reconstructing the eruptive history of a monogenetic volcano through a combination of fieldwork and geophysical surveys: the example of Puig d'Àdri (Garrotxa Volcanic Field). J Geol Soci 173(6):875
Peregi Z (2003) Geological map of Libya scale : 250,000 for AL HARUJ AL ABYAD NG 33–8. Geological Institute of Hungaryand Industrial Research Centre, Budapest–Tripoli, p 240
Petronis M, Delcamp A, Wyk V, de Vries B (2013) Magma emplacement into the Lemptégy scoria cone (Chaîne Des Puys, France) explored with structural, anisotropy of magnetic susceptibility, and Paleomagnetic data. BV 75:753
Petronis M, Brister AR, Rapprich V, Wyk V, de Vries B, Lindline J, Misurec J (2015) Emplcament history of the Trosky basanitic volcano (Czech Republic): paleomegnetic, rock magnetic, petrologic, and anisotropy of magnetic susceptibility evidence for linger growth of a monogenetic volcano. J Geosci 60:129–147
Petronis M, Valenta J, Rapprich V, Lindline J, Heizler M, Wyk V, de Vries B, Shields S, Balek J, Fojtíková L, Tábořík P (2018) Emplacement history of the Miocene Zebín Tuff Cone (Czech Republic) revealed from ground geophysics, anisotropy of magnetic susceptibility, paleomagnetic, and $^{40}Ar/^{39}Ar$ geochronology data. Geochem Geophys Geosyst. https://doi.org/10.1029/2017GC007324
Pinkerton H, Sparks RSJ (1976) The 1975 sub-terminal lavas, Mount Etna: a case history of the formation of a compound lava field. J Volcanol Geotherm Res 1(2):167–182
Pioli L, Erlund E, Johnson E, Cashman K, Wallace P, Rosi M, Delgado Granados H (2008) Explosive dynamics of violent Strombolian eruptions: the eruption of Parícutin Volcano 1943–1952 (Mexiko). Earth Planet Sci Lett 271:359–368
Poblete MA (1995) El relieve volcánico del Campo de Calatrava (Ciudad Real). Ph.D.Thesis, OviedoUniv, Oviedo, p 145
Pola A, Macías JL, Osorio-Ocampo S, Sosa-Ceballos G, Garduño-Monroy VH, Martínez-Martínez J (2015) El Estribo volcanic complex: evolution from a shield volcano to a cinder cone, Pátzcuaro Lake, Michoacán. México J Volcanol Geotherm Res 303:130–145. https://doi.org/10.1016/j.jvolgeores.2015.07.032
Polacci M, Corsaro RA, Andronico D (2003) Coupled textural and compositional characterization of basaltic scoria: insights into the transition from Strombolian to fire fountain activity at Mount Etna, Italy. Geology 34:201–204

Porritt LA, Russell JK, Quane SL (2012) Pele's tears and spheres: examples from Kilauea Iki. Earth Planet Sci Lett 333–334:171–180

Re G, White JDL, Ort MH (2015) Dikes, sills, and stress-regime evolution during emplacement of the Jagged Rocks complex, Hopi Buttes Volcanic field, Navajo Nation, USA. J Volcanol Geotherm Res 295:65–79

Riedel C, Ernst GGJ, Riley M (2003) Controls on the growth and geometry of pyroclastic constructs. J Volcanol Geotherm Res 127(1–2):121–152

Risso C, Prezzi C, Julia Orgeira M, Nullo F, Margonari L, Nemeth K (2015) Inverse steptoes in Las Bombas volcano, as an evidence of explosive volcanism in a solidified lava flow field. Southern Mendoza-Argentina. J S Am Earth Sci 63:360–374

Roobol MJ, Camp VE (1991) Geologic map of the Cenozoic lava field of Harrat Kishb, Kingdom of Saudi Arabia at scale 1:250,000. Saudi Arabian Directorate General of Mineral Resources, p 34

Rooney TO, Hart WK, Hall CM, Ayalew D, Ghiorso MS, Hidalgo P, Yirgu G (2014) Peralkaline magma evolution and the tephra record in the Ethiopian Rift. Contrib Mineral Petrol 164:407–426

Rosi M, Bertagnini A, Harris AJL, Pioli L, Pistolesi M, Ripepe M (2006) A case history of paroxysmal explosion at Stromboli: timing and dynamics of the April 5, 2003 event. Earth Plan Sci Lett 243:594–606

Ross PS, White JDL, Zimanowski B, Büttner R (2008) Rapid injection of particles and gas into non-fluidized granular material, and some volcanological implications. Bull Volcanol 70(10):1151–1168

Ross PS, Delpit S, Haller MJ, Németh K, Corbella H (2011) Influence of the substrate on maar–diatreme volcanoes—an example of a mixed setting from the Pali Aike volcanic field, Argentina. J Volcanol Geotherm Res 20:253–271

Ross PS, White JDL, Valentine GA, Latutrie B (2018) Distinguishing magmatic from phreatomagmatic pyroclastic deposits at prehistoric mafic maar volcanoes. Italian Society of volcanology, Naples, Italy

Rossetti LM, Lima EF, Waichel BL, Scherer CM, Barreto CJ (2014) Stratigraphical framework of basaltic lavas in Torres Syncline main valley, southern Parana-Etendeka Volcanic Province. J S Am Earth Sci 56:409–421

Rowland SK, Walker GP (1987) Toothpaste lava: characteristics and origin of a lava structural type transitional between pahoehoe and aa. Bull Volcanol 49(4):631–641

Rowland S, Jurado-Chichay Z, Ernst G, Walker G (2009) Pyroclastic deposits and lava flows from the 1759–1774 eruption of El Jorullo, Mexico: aspects of 'violent Strombolian' activity and comparison with Parícutin. In: Thordarson T, Self S, Larsen G, Rowland S, Hoskuldsson A (eds) Studies in volcanology: the legacy of George Walker. Vol. 2 of Special Publications of IAVCEI. Geological Society, London, pp 105–128

Sable JE, Houghton BF, Del Carlo P, Coltelli M (2006) Changing conditions of magma ascent and fragmentation during the Etna 122 BCE basaltic Plinian eruption: evidence from clast microtextures. J Volcanol Geotherm Res 158(3):333–354

Said R (1962) The geology of Egypt, Amsterdam. Elsevier Publ. Co, Oxford, p 37

Said R (1990) The geology of Egypt. A.A. Balkema, Rotterdam, p 734

Saucedo R, Macías JL, Ocampo-Díaz YZE, Gómez-Villa W, Rivera-Olguín E, Castro-Govea R, Sánchez-Núñez JM, Layer PW, Hernández JR, Carrasco-Núñez G (2017) Mixed magmatic—phreatomagmatic explosions during the formation of the Joya Honda maar, San Luis Potosí, Mexico. Geol Soc Spec Pub 446:255–279

Schaefer CJ, Kattenhorn SA (2004) Characterization and evolution of fractures in low volume pahoehoe lava flows, eastern Snake River Plain, Idaho. Geol Soc Am Bull 116:3–4

Schilling JG, Kingsley RH, Hanan BB, McCully BL (1992) Nd–Sr–Pb isotopic variations along the Gulf of Aden—evidence for Afar mantle plume continental lithosphere interaction. J Geophys Res Solid Earth 97:10927–10966

Schmincke HU, Sumita M (2010) Geological evolution of the Canary Islands. A young volcanic archipelago adjacent to the Old African Continent. Gorres-Druckerei und Verlag GMBH, Koblenz

Schumacher R, Schmincke HU (1991) The lateral facies of ignimbrite at Laacher See volcano. Bull Volcanol 52:271–285

Sehim A (1993) Wrenching tectonics in Egypt. J Geol 37–1:335–372

Self S, Kienle J, Huot JP (1998) Ukinrek Maars, Alaska, II. Deposits and formations of the 1977 craters. J Volcanol Geotherm Res 7(1–2):39–65. https://doi.org/10.1016/0377-0273(80)90019-0

Self S, Thordarson T, Keszthelyi L, Walker GPL, Hon K, Murphy MT, Finnemore S (1996) A new model for the emplacement of Columbia River basalts as large, inflated pahoehoe lava flow fields. Geophys Res Lett 23(19):2689–2692

Shaw HR, Wright TL, Peck DL, Okamura R (1968) The viscosity of basalticmagma; an analysis of field measurements in Makaopuhi lava lake. Hawaii Am J Sci 266(4):225–264

Shea T, Houghton BF, Gurioli L, Cashman KV, Hamnar JE, Hobden BJ (2010) Textural studies of vesicles in volcanic rocks: an integrated methodology. J Volcanol Geotherm Res 190:271–289

Sheth H, Meliksetian K, Gevorgyan H, Israyelyan A, Navasardyan G (2015) Intracanyon basalt lavas of the Debed River (northern Armenia), part of a Pliocene-Pleistocene continental flood basalt province in the south Caucasus. J Volcanol Geotherm Res 295:1–15

Smith IEM, Nemeth K (2017) Source to surface model of monogenetic volcanism; a critical review. Sp Publ Geol Soc Lond 446(1):1–28

Sohn YK (1996) On traction-carpet sedimentation. J Sed Res 67:502–509

Sohn YK, Chough SK (1990) Depositional processes of the Suwolbong tuff ring, Cheju Island (Korea). Sedimentology 36(5):837–855

Sohn YK, Chough SK (1992) The Ilchulbong tuff cone, Cheju Island, South Korea. Sedimentology 39(4):523–544

Sottili G, Taddeucci J, Palladino DM, Gaeta M, Scarlato P, Ventura G (2009) Subsurface dynamics and eruptive styles of maars in the Colli Albani Volcanic District, Central Italy. J Volcanol Geotherm Res 180:189–202

Sottili G, Taddeucci J, Palladino D (2010) Constraints on magma–wall rock thermal interaction during explosive eruptions from textural analysis of cored bombs. J Volcanol Geotherm Res 192:27–34

Stovall WK, Houghton BF, Gonnermann H, Fagents SA, Swanson DA (2011) Eruption dynamics of Hawaiian-style fountains: the case study of episode 1 of the Kīlauea Iki 1959 eruption. Bull Volcanol 73(5):511–529

Stovall WK, Houghton BF, Hammer JE, Fagents SA, Swanson DA (2012) Vesiculation of high fountaining Hawaiian eruptions: episodes 15 and 16 of 1959 Kīlauea Iki. Bull Volcanol 74:441–455

Sumner JM (1998) Formation of clastogenic lava flows during fissure eruption and scoria cone collapse: the 1986 eruption of Izu-Oshima Volcano, eastern Japan. Bull Volcanol 60(3):195–212

Sumner JM, Branney MJ (2002) The emplacement of a remarkable heterogeneous, chemically zoned and locally lava-like rheomorphic ignimbrite: 'TL' on Gran Canaria. J Volcanol Geotherm Res 115:109–138

Sumner J, Blake S, Matela R, Wolff J (2005) Spatter. J Volcanol Geotherm Res 142:49–65

Sun SS, McDonough WF (1989) Chemical and isotopic systematics of oceanic basalts: implications for mantle composition and processes. In: Saunders AD, Norry MJ (eds) Magmatism in the ocean basins, vol 42. Geol Soci Lond Spec Publs, pp 313–345

Thordarson T, Self S (1993) The Laki (Skaftár Fires) and Grímsvötn eruptions in 1783–1785. Bull Volcanol 55:233–263

Ureta G, Németh, K, Aguilera F, Vilches M, Aguilera M, Torres I, Sepúlveda J, Scheinost A, González R (2020a) An overview of the mafic and felsic monogenetic neogene to quaternary volcanism in the central Andes, northern Chile (18-28°Lat.S). In: Németh K (ed) Volcanoes - updates in volcanology. IntechOpen, Rijeka, Croatia. https://doi.org/10.5772/intechopen.93959

Ureta G, Aguilera F, Németh K, Inostroza M, González C, Zimmer M, Menzies A (2020b) Transition from small-volume ephemeral lava emission to explosive hydrovolcanism: The case of Cerro Tujle maar, northern Chile. JS Am Earth Sci 104:102885

Ureta G, Németh K, Aguilera F, Kósik S, González R, Menzies A, González C, James D (2021) Evolution of a magmatic to a phreatomagmatic volcanic system: The birth of a monogenetic volcanic field, Tilocálar volcanoes, northern Chile. J Volcanol Geotherm Res 414:107243

Valentine G, Krogh K (2006) Emplacement of shallow dikes and sills beneath a small basaltic volcanic centre—the role of pre-existing structure (Paiute Ridge, southern Nevada, USA). Earth Planet Sci Lett 246:217–230

Valentine GA, Keating GN (2007) Eruptive styles and inferences about plumbing systems at Hidden Cone and Little Black Peak scoria cone volcanoes (Nevada, U.S.A.). Bull Volcanol 70(1):105–113

Valentine GA, Perry FV (2007) Tectonically controlled, timepredictable basaltic volcanism from a lithospheric mantle source (central Basin and Range Province, USA). Earth Planet Sci Lett 261:201–216

Valentine GA, Gregg TKP (2008) Continental basaltic volcanoes — processes and problems. J Volcanol Geotherm Res 177:857–873

Valentine GA, White JDL (2012) Revised conceptual model for maar-diatremes: subsurface processes, energetics, and eruptive products. Geol 40:1111–1114

Valentine G, Zhang D, Robinson BA (2002) Modelling complex, nonlinear geological processes. Annual Rev Earth Planetary Sci 30:35–64

Valentine G, Krier D, Perry F, Heiken G (2005) Scoria cone construction mechanisms, Lathrop Wells volcano, southern Nevada, USA. Geology 33(8):629–632

Valentine GA, Perry FV, Krier DJ, Keating GN, Kelley RE, Cogbill AH (2006) Small volume basaltic volcanoes: eruptive products and processes, and post-eruptive geomorphic evolution in Crater Flat (Pleistocene), southern Nevada. Geol Soc Am Bull 118:1313–1330. https://doi.org/10.1130/B25956.1

Valentine GA, Krier DJ, Perry FV, Heiken G (2007) Eruptive and geomorphic processes at the Lathrop Wells scoria cone volcano. J Volcanol Geotherm Res 161:57–80

Valentine GA, Graettinger AH, Sonder I (2014) Explosion depths for phreatomagmatic eruptions. Geophys Res Lett 41(9):3045–3051

Valentine GA, White JDL, Ross PS, Graettinger AH, Sonder I (2017) Updates to concepts on phreatomagmatic maar-diatremes and their pyroclastic deposits. Front Earth Sci 5:68

Vergniolle S, Mangan M (2000) Hawaiian and Strombolian eruptions. In: Sigurdsson H (ed) Encyclopedia of volcanoes. Academic, San Diego, pp 447–461

Vespermann D, Schmincke UH (2000) Scoria cones and tuff rings. In: Sigurdsson H (ed) Encyclopedia of volcanoes. Academic, San Diego, pp 683–694

Volker F, Altherr R, Jochum KP, McCulloch MT (1997) Quaternary volcanic activity of the southern Red Sea: new data and assessment of models on magma sources and afar plume lithosphere interaction. Tectonophys 278:15–29

Walker GPL (1971) Compound and simple lava flows and flood basalts. Bull Volcanol 35(3):579–590. https://doi.org/10.1007/bf02596829

Walker GPL (1973) Explosive volcanic eruptions—a new classification scheme. Geol Rundsch 62(2):431–446

Walker GP (2000) Basaltic volcanoes and volcanic systems. In: Sigurdsson H, Houghton B, McNutt S, Rymer H, Stix J (eds) The encyclopedia of volcanoes. Academic Press, pp 283–289

Walker GPL, Croasdale R (1971) Characteristics of some basaltic pyroclastics. Bull Volcanol 35:303–317

White JDL (1990) Depositional architecture of a maar-pitted playa-sedimentation in the Hopi Buttes volcanic field, Northeastern Arizona, USA. Sed Geol 67(1–2):55–84

White JDL (1991a) Maar-diatreme phreatomagmatism at Hopi Buttes, Navajo Nation (Arizona). USA Bull Volcanol 53:239–258

White JDL (1991b) The depositional record of small, monogenetic volcanoes within terrestrical basins. In: Fisher RV, Smith GA (eds) Sedimentation in volcanic settings. Society for Sed. Geol, Tulsa, pp 155–171

White JDL, Ross PS (2011) Maar-diatreme volcanoes: a review. J Volcanol Geotherm Res 201:1–29

White JDL, Valentine GA (2016) Magmatic versus phreatomagmatic fragmentation: absence of evidence is not evidence of absence. Geosphere 12(5):1478–1488. https://doi.org/10.1130/GES01337.1

Winchester JA, Floyd PA (1976) Geochemical magma type discrimination: application to altered and metamorphosed basic igneous rocks. Earth Planet Sci Lett 28:459–469

Winter C, Breitkreuz C, Lapp M (2008) Textural analysis of a Late Palaeozoic coherent–pyroclastic rhyolitic dyke system near Burkersdorf (Erzgebirge, Saxony, Germany). Geol Soc Spec Publ Lond 302:199–221

Wohletz KH (1986) Mechanisms of hydrovolcanic pyroclasts formation: grain size, scanning electron microscopy, and experimental studies. J Volcanol Geotherm Res 17:31–63

Wohletz K, Heiken G (1992) Volcanic ash, 2nd edn. University of California Press, p 432

Wohletz KH, Sheridan MF (1983) Hydrovolcanic explosions II: evolution of basaltic tuff rings and tuff cones. Am J Sci 283:385–413

Wolff JA, Sumner JM (2000) Lava fountains and their products. In: Sigurdsson H, Houghton B, McNutt S, Rymer H, Stix J (eds) Encyclopedia of volcanoes. Academic, San Diego, pp 321–330

Wolff JA, Ellwood BB, Sachs SD (1999) Anisotropy of magnetic susceptibility inwelded tuffs: application to awelded-tuff dyke in the tertiary Trans-Pecos Texas volcanic province, USA. Bull Volcanol 51(4):299–310. https://doi.org/10.1007/BF01073518

Wood CA (1980) Morphometric evolution of cinder cones. J Volcanol Geotherm Res 7:387–413

Yasui M, Koyaguchi T (2004) Sequence and eruptive style of the 1783 eruption of Asama Volcano, central Japan: a case study of an andesitic explosive eruption generating fountain-fed lava flow, pumice fall, scoria flow and forming a cone. Bull Volcanol 66(3):243–262

Zimanowski B, Buettner R (2003) Phreatomagmatic explosions in subaqueous volcanism. In: White JDL, Smellie JL, Clague DA (eds) Explosive subaqueous volcanism. Geophysical monographs. Amer Geophys Union, Washington, DC, pp 51–60

Zimanowski B, Büttner R, Lorenz V, Häfele HG (1997) Fragmentation of basaltic melt in the course of explosive volcanism. J Volcanol Geotherm Res 102:803–814